Numerical Solutions of Laplace's Equation for Various Physical Situations

by

Colin J. Vendromin

A THESIS SUBMITTED IN PARTIAL FULFILMENT OF
THE REQUIREMENTS FOR THE DEGREE OF

MASTER OF SCIENCE

in

The Faculty of Mathematics and Sciences

Department of Physics

BROCK UNIVERSITY

September 11, 2017

In presenting this thesis in partial fulfilment of the requirements for an advanced degree at the Brock University, I agree that the Library shall make it freely available for reference and study. I further agree that permission for extensive copying of this thesis for scholarly purposes may be granted by the head of my department or by his or her representatives. It is understood that copying or publication of this thesis for financial gain shall not be allowed without my written permission.

(Signature) _____

Department of Physics

Brock University
St.Catharines, Canada

Date _____

Abstract

There are two projects in this thesis. In the first project, a general method is introduced to numerically calculate the resistance of truncated resistors in cylindrical coordinates, with non-constant cross-sectional area. The problem of finding the resistance of a truncated conical resistor is given in some introductory textbooks as a simple problem. The textbook method is flawed however, and leads to the wrong answer. The textbook method assumes that the electric potential distribution inside the truncated cone is approximately equivalent to a cylindrical resistor. This assumption ignores the constricting affect that the boundary of the truncated conical resistor has on the electric potential inside. The deformation of the electric field is not accounted for by excess charge or changing magnetic fields, instead it is the result of a derivative operation called the shear of the field. Numerical solutions for the resistance of truncated conical, ellipsoidal, and hyperboloidal resistors are presented as a function of a/b, where a is the radius of the smallest cross-sectional area and b is radius of the largest. It was found that the textbook solution always underestimates the numerical value of the resistance.

In the second project, dielectric breakdown clusters were grown with a stochastic two dimensional Dielectric Breakdown Model (DBM) on a honeycomb, square, and triangle lattice, as well as on a random distribution of nodes. On the regular lattices the number of nearest neighbours was a constant at all lattice sites. For a random distribution of nodes there was variation in the number of nearest neighbours at different nodes. Some percentage of the nodes were isolated from the rest of the distribution, because they had 0 nearest neighbours. Distributions of nodes in which many of the nodes had 0 nearest neighbours indicated a medium with high density fluctuations. The motivation for this work was to study the relationship between the fractal dimension of the dielectric breakdown clusters and the number of nearest neighbours, and the density variation of the medium. The singularity spectra, $f(\alpha)$, were calculated for the clusters, as well as their fractal dimension using box counting, and sandbox methods. It was found that the dielectric breakdown model produces monofractal clusters. As such, the dimension of the clusters can be represented by a single fractal dimension. In the DBM, the probability of a perimeter site connecting to the cluster is proportional to the strength of the local electric field raised to an exponent, η. If η is a large positive number then perimeter sites which feel a stronger electric field are more likely to connect to the cluster. Increasing η produces clusters which resemble lightning, with a fractal dimension lower than the dimension of the lattice. Similarly increasing the percentage of isolated nodes decreases the fractal dimension.

Contents

List of Tables

List of Figures

Acknowledgements

I would like to acknowledge my supervisors Dr. David Crandles, and Dr. Shyamal Bose for their unwavering support, patience, and encouragement.

Chapter 1

Introduction

This thesis involves solving the Laplace equation numerically for various physical situations.

The first project investigates the electrical resistance of solid resistors which have a cross-sectional area that varies along the length of the resistor. In such cases, to get an accurate result, one must consider the potential everywhere inside the resistor, then calculate the resistance from the total current.

The second project implements the Dielectric Breakdown Model (DBM) to study the fractal dimension of electrical discharge in an insulator. The DBM is a modification of Diffusion Limited Aggregation (DLA) [1]. DLA is a stochastic process that begins by a seed particle being placed at the center of a lattice. Another particle, starting from a large distance away, performs a random walk until it arrives at one of the lattice sites neighbouring an already occupied site. Then the random walk is stopped, and another particle is sent on a random walk starting from far away. This process continues until a large cluster of particles is formed. In the DBM a seed particle is placed at the center of a lattice. The value of an electric potential for an occupied site is set to 0V, and at a far away boundary the potential is 1V. The potential is then numerically solved on every lattice site with these boundary conditions. Each perimeter site to the occupied sites is assigned a probability of occupation according to the local strength of the electric field (gradient of the potential) raised to an exponent η. A perimeter site becomes occupied if another random number uniformly distributed between 0 and 1 is less than the occupation probability for the site. The addition of another particle changes the electric field configuration, and so the potential must be re-calculated after each particle is added.

Both projects require the numerical determination of a scalar potential, embedded in some geometry, and subject to non-trivial boundary conditions.

1.1 Electrical Resistance of Solids

Some introductory textbooks to electromagnetism include the problem of finding the resistance of a truncated cone, as an example for the application of the formula $R = \rho L/A$ [2], [3], where ρ is the resistivity, L is the length, and A is the cross sectional area. The solution to the problem is given by $R = \rho L/\pi ab$, where a is the radius of the smallest cross-sectional area and b is the radius of the largest. The textbook method considers the solid resistor as a construction of infinitesimal volumes with cross sectional area, $A(z)$, and infinitesimal height, dz (Fig. 1.1). One can find the resistance, dR, of each volume, and then integrate to find the total resistance, $R = \rho \int dz/A(z)$. The implicit assumption in this method is that one can treat the boundary between each infinitesimal volume as a horizontal electrode surface, or equipotential. The cross sectional area of one infinitesimal volume, $A(z)$, will be larger or smaller than, and not entirely cover, the next one, $A(z + dz)$. The electric field is perpendicular to the electrode surfaces. Due to the overlapping of resistive layers $A(z)$ and $A(z + dz)$, charge will build up at the interface between the exterior and interior of the resistive layers. This causes an overestimation of the total current, and an underestimation of the resistance.

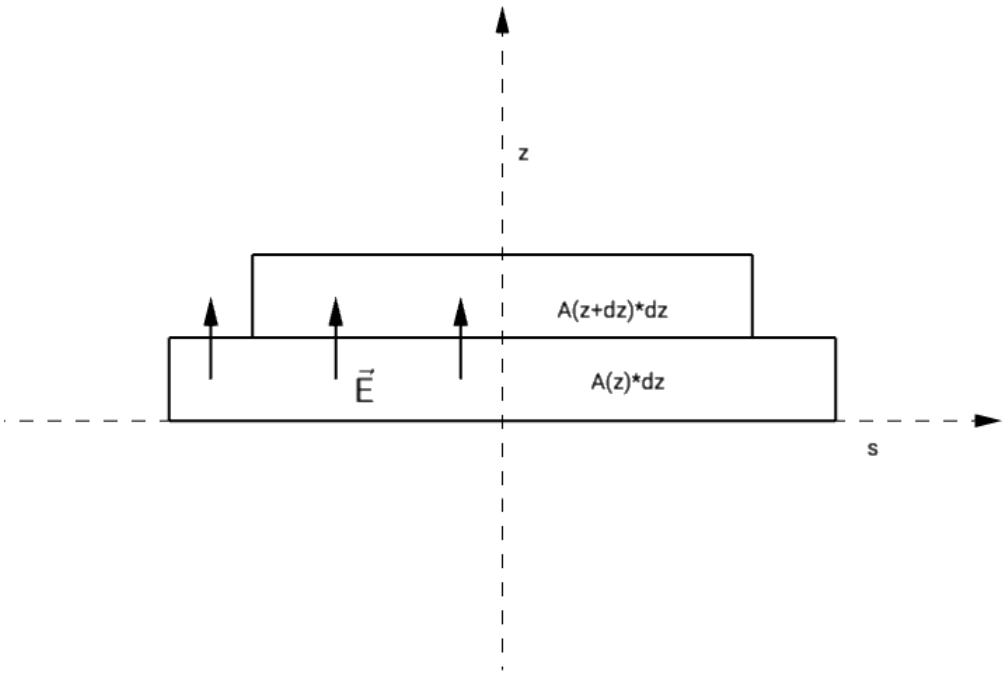

Figure 1.1: This is an image of two cylindrical resistive layers, with volume, dV, and cross sectional area, $A(z)$, that construct a solid resistor in cylindrical coordinates (s, θ, z). Subsequent resistive layers do not perfectly overlap, causing the electric field lines to escape through the boundary.

This solution is only an approximate solution for values of $a/b \approx 1$. The underlying assumption is that the equipotential surfaces are flat like in a cylindrical resistor, and the current density is constant. J.D. Romano and R.H. Price [3] were the first researchers to calculate the resistance of the truncated cone without using a constant current density approximation. Instead, they computed the electric potential, Φ, everywhere inside a truncated cone, and found the current density by $\vec{J} = -\sigma\vec{\nabla}\Phi$, where σ is the electrical conductivity ($\sigma = 1/\rho$). Then the resistance is $R = \Delta\Phi/I$, where $I = \int \vec{J} \cdot d\vec{a}$. For $a/b = 0.5$, and $L/b = 1$, they found that their numerical solution was about 9% larger than the approximate solution given in textbooks [2], which was much greater than the error of their calculation – approximately 0.1%. The numerical solution reduces to solving Laplace's equation (section 2.1) for a scalar electric potential everywhere inside the solid resistor, subject to the boundary conditions that the electric field is parallel to the sides of the resistor, and constant on the truncation surfaces. If the electric field were not parallel to the sides of the resistor this would imply some component of the electric field can escape through the sides of the resistor, due to charge build up, which is assumed to not occur. Once the potential is known everywhere, the total current can be found by integrating the normal component of the current density over either electrode surface. The truncated cone is shown in Fig. 1.2. They did their resistance calculation for when the radius of the smaller electrode, where the cone was truncated, was half the diameter of the larger electrode.

This project generalizes the work done by J.D. Romano and R.H. Price by numerically calculating the resistance of truncated conical, ellipsoidal and hyperboloidal resistors as a function of a/b (Fig. 1.2).

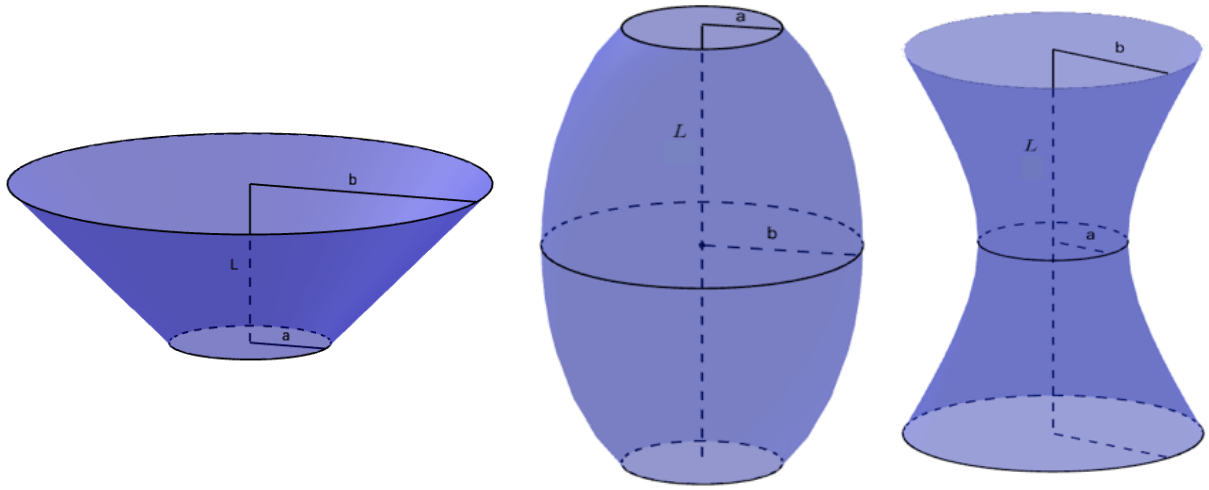

Figure 1.2: Geometry of the truncated conical, ellipsoidal, and hyperboloidal solid resistors. The light blue circular disks are electrode contact surfaces, and are formed by the intersection of two horizontal planes with the solid. The circular cross-sections with radii a and b are considered as constant potential surfaces, with $a \leq b$.

It is useful to think of the total resistance as a sum of two resistances, $R = R_{bulk} + R_{spreading}$ [4]. The bulk resistance (textbook solution) is calculated assuming constant current density (cylindrical resistor), and the spreading resistance term accounts for the bending of current flow lines due to $a \neq b$ (deviation from cylindrical resistor). When $a/b << 1$ the current flow lines exhibit extensive bending, and the spreading resistance term will contribute more to the total resistance causing the assumption of constant current density to be less accurate. The deformation of the electric field (bending of current flow lines) is not accounted for by excess charge or changing magnetic fields, instead it is the result of a derivative operation called the shear of the field. It can be shown[5] that the nine components of the gradient $\vec{\nabla}\vec{E}$ of the electric field $\vec{E}$ can be written in terms of a symmetric, anti-symmetric, and trace-free matrix

$$\frac{\partial E_i}{\partial x^j} = S(\vec{E})_{ij} - \frac{1}{2}\epsilon_{ijk}\left(\vec{\nabla} \times \vec{E}\right)_k + \frac{1}{3}\delta_{ij}\left(\vec{\nabla} \cdot \vec{E}\right). \tag{1.1}$$

These components form a 3×3 matrix, where $x^i = [x, y, z]$ are the Cartesian coordinates. The symbols δ_{ij} and ϵ_{ijk} are the Kronecker delta and Levi-Civita symbols, and $S(\vec{E})_{ij}$ is a trace-free

symmetric matrix called the shear of $\vec{E}$,

$$S(\vec{E})_{ij} \equiv \frac{1}{2}\left(\frac{\partial E_i}{\partial x^j} + \frac{\partial E_j}{\partial x^i}\right) - \frac{1}{3}\delta_{ij}\left(\vec{\nabla}\cdot\vec{E}\right). \tag{1.2}$$

For electrostatic problems in which the electric field has no curl or divergence, the only components which are non-zero in (1.1) come from the shear. In cylindrical coordinates (s, ϕ, z) with a divergence-less and curl-less electric field, it can be shown [5] the shear of $\vec{E}$ is

$$S(\vec{E}) = \begin{bmatrix} \frac{\partial E_s}{\partial s} & 0 & \frac{\partial E_s}{\partial z} \\ 0 & \frac{E_s}{s} & 0 \\ \frac{\partial E_z}{\partial s} & 0 & \frac{\partial E_z}{\partial z} \end{bmatrix} \tag{1.3}$$

where the off-diagonal elements have been simplified using $\vec{\nabla}\times\vec{E} = 0$, and it is assumed that the field is ϕ-independent. To understand the physical interpretation of the shear, consider a cylindrical resistor with its axis parallel to the z-axis in cylindrical coordinates. A constant electric field, $\vec{E} = E\hat{z}$, exists between the electrodes. Substituting the electric field for a cylindrical resistor into (1.3) gives a value of 0 for every element in the shear matrix. This means a cylindrical element of current density ($\vec{J} = \frac{1}{\rho}\vec{E}$) passes from one electrode to the next, parallel to the z-axis, with no deformation. In general the components of the electric field are a function of (s, z), and have an $\hat{s}$ component. Then, the shear represents the rate at which a cylindrical element of current density deforms as it passes between electrodes.

1.2 Dielectric Breakdown

There has been considerable interest and effort in classifying natural phenomena such as electrodeposition, mineral deposition, and dielectric breakdown (Lichtenberg figures, capacitor failure, and lightning). Lichtenberg figures are branched electrical discharge patterns inside or on the surface of electrically insulating materials. These phenomenon are examples of fractals, and can be modeled by a process called Diffusion-Limited-Aggregation (DLA) [1]. DLA is a stochastic process where particles are joined together to form an overall cluster. In the case of dielectric breakdown, L.

Niemeyer et al [6] developed a Dielectric Breakdown Model (DBM) as a DLA model which adds electrons to the cluster depending on a local electric field. The probability of an electron occupying a neighbouring site to the cluster depends on the strength of the local electric field raised to some exponent, η, (Eq. 2.50). In general, the relationship between probability and field could be a power series expansion of the field. The probability would then depend on a combination of linear and non-linear terms. We consider both linear and non-linear discharge models, with $\eta = 0.5, \eta = 1$, and $\eta = 2$. The purpose of η is to classify the medium in which breakdown occurs. Setting η equal to 1 models a standard Ohmic resistor, valid for small electric fields. For η greater than or less than 1 the medium becomes non-linear, such that the conduction of electrons across nearest neighbour bonds depends non-linearly on the local electric field. The fractal dimension (see section 2.9) is defined as the exponent D in the scaling relationship, $N(L) \sim L^D$, where $N(L)$ is the number of sites which belong to the fractal in some circle of radius L.

Researchers have studied the impact that η has on the fractal dimension of the resulting cluster, in 2D [6] or 3D [7], for various physical boundary conditions, such as radial discharges [6],[7] and thin capacitors [8]. Increasing η from 0 generates increasingly sparse clusters with a fractal dimension less than the dimension of the lattice. L. Niemeyer et al. in 1984 [6] studied their DBM with computer simulations. They considered a 2D square lattice which has one electrode at the center, and a second electrode modeled as a circular boundary far away. The electrons move from the first electrode, at the center of the lattice, towards the electrode boundary, due to the electric field between the electrodes. Electrons are more likely to move to nearest neighbour sites if the local electric field across the bond is strong. In the dielectric breakdown model the probability an electron will move across a bond is proportional to the strength of the electric field raised to an exponent, η. If $\eta = 0$ the movement of the electron is independent of the field, and one recovers a purely random walk. However, if the exponent is large the trajectory of the electron approaches a straight line between the two electrodes. Once a conducting path has been created between the electrodes the process of growth stops. The global breakdown cluster resembles actual electron discharge patterns observed in experiments and nature. L. Niemeyer et al. classified the global structure of the computer generated patterns by calculating their fractal dimension. They also varied the exponent in the relation between probability and local electric field, and recorded how the fractal

dimension changed.

In this project, dielectric breakdown clusters are grown on a honeycomb, square, and triangle lattice, as well as on a random distribution of nodes. For regular lattice types the number of nearest neighbours is constant for every site in the lattice. For a random distribution of nodes, the total number of nodes is the same as the square lattice, but the gaps between nodes are not all the same size. The number of nodes within a neighbourhood will vary depending on the location in the distribution. Some percentage of the nodes are isolated from the rest of the distribution, because they have 0 nearest neighbours. Distributions of nodes in which many of the nodes have 0 nearest neighbours are interpreted as a locally less-dense medium than the square lattice. If a node has 0 neighbours, then another node will have more than 4 neighbours to ensure the total number of nodes is constant. The motivation for this work is to study the relationship between the fractal dimension of the dielectric breakdown clusters and the number of nearest neighbours, and the density of the medium.

In addition, we will study the self-similarity (see section 2.9) of the clusters over multiple length scales. The clusters will be studied with a multifractal analysis by calculating their singularity spectra $f(\alpha)$ (see subsection 2.9.1). If the distribution of mass in the fractal is uniform, then the number of sites $N(L)$ which belong to the cluster within some circle of radius L is the same for all regions. If the distribution of mass is non-uniform, then the value of $N(L)$ will change depending on the region of the cluster. In each region $N(L)$ scales with L according to the power law relationship, $N(L) \sim L^{\alpha}$, where α is the singularity strength of the region in the cluster. In general, a cluster will exhibit a distribution of α values, where $\Delta\alpha = \alpha_{max} - \alpha_{min}$ gives a measure of the multifractality. A multifractal cluster contains many values of α. For a monofractal, every region of the cluster scales with the same α, and there is only one fractal dimension. Although α depends on the region in the cluster, many sites will have approximately the same α value. In general, the number of sites within a neighborhood ϵ which have approximately the same value of α scales with ϵ according to $N_{\alpha}(\epsilon) \sim \epsilon^{f(\alpha)}$, where $f(\alpha)$ is the fractal dimension of the subset of lattice sites characterized by the exponent α. The function $f(\alpha)$ is a concave function with a maximum value equal to the fractal dimension of the cluster. Another interpretation of $f(\alpha)$ is to think of it as a measure of the likelihood that an exponent α will be found in the cluster [9]. For a monofractal, only one value of

α is found in the cluster, and there will only be one point in the $f(\alpha)$ curve.

Chapter 2

Methods

In this section the numerical methods and techniques that were used to obtain the results of this thesis will be discussed.

2.1 The Laplace Equation

This section is inspired by chapter 5 in the book "Electromagnetism" by Pollack and Stump [10].

In electrostatic problems, where the curl of the electric field is zero $\vec{\nabla} \times \vec{E} = 0$, the electric field can be written as the gradient of a scalar potential

$$\vec{E} = -\vec{\nabla}\Phi. \tag{2.1}$$

Maxwell's equation for the divergence of the electric field is $\vec{\nabla} \cdot \vec{E} = \rho'/\epsilon_0$, where ρ' is the charge density, and ϵ_0 is the permittivity of free space. Replacing the electric field in Maxwell's equation with (2.1) gives

$$\nabla^2\Phi = -\rho'/\epsilon_0. \tag{2.2}$$

This equation is called Poisson's equation. When there is no charge density Poisson's equation becomes Laplace's equation,

$$\nabla^2\Phi = 0. \tag{2.3}$$

Solving Laplace's equation in a domain with the appropriate boundary conditions on the electric field gives a unique solution for the electric field (see section 2.1.2).

2.1.1 Boundary Conditions

There are some boundary conditions that the electric field $\vec{E}$ must obey, which result from evaluating Maxwell's equations near a surface. Consider an electric field inside a domain with volume V that has a surface denoted by S. Construct a rectangular prism with cross sectional area $A = L \times W$ and height ϵ. Put the prism on the surface S such that it extends an infinitesimal amount, $\epsilon/2$, on either side of S, and A is parallel to a tangent plane on S. If there is a surface charge density σ' on S, then calculating the electric field flux through the rectangular prism will measure the total charge inside

$$\oint_S \vec{E} \cdot d\vec{a} = \frac{1}{\epsilon_o}\sigma' A \tag{2.4}$$

where $\sigma' A$ is the total charge inside the rectangular prism. The vector $d\vec{a}$ is normal to A, and $\vec{E} \cdot d\vec{a}$ is the normal component of the electric field to A. In the limit as ϵ goes to zero (i.e. as the rectangular prism straddles the surface closer), the integral in (2.4) can be approximated by

$$\lim_{\epsilon \to 0} \oint_S \vec{E} \cdot d\vec{a} \to E^{\perp}_{above} A - E^{\perp}_{below} A. \tag{2.5}$$

Therefore the normal component of the electric field is discontinuous by an amount σ'/ϵ_o at any boundary,

$$E^{\perp}_{above} - E^{\perp}_{below} = \frac{1}{\epsilon_o}\sigma'. \tag{2.6}$$

In the case when there is no surface charge density, then $\sigma' = 0$ in (2.6), and the normal component is continuous across the boundary. In terms of the electric potential Φ (2.6) can be restated as

$$\frac{\partial \Phi_{above}}{\partial n} - \frac{\partial \Phi_{above}}{\partial n} = -\frac{1}{\epsilon_o}\sigma' \tag{2.7}$$

where n is the direction normal to the surface S.

There is also a boundary condition on the parallel component of E. Consider a thin rectangular loop with a perimeter $P = 2(l + \epsilon)$. The sides of the loop with length l are parallel to a tangent vector on S. The loop is positioned in S such that the sides with length ϵ extend a distance of $\epsilon/2$

above and below S. In the absence of any magnetic fields the curl of E must be zero

$$\oint_{loop} \vec{E} \cdot d\vec{l} = 0. \tag{2.8}$$

The vector $d\vec{l}$ is a small segment of the path on the loop. The product $\vec{E} \cdot d\vec{l}$ is the component of the electric field which is parallel to the loop. In the limit as ϵ goes to zero, the perimeter of the loop approaches $P = 2l$, and the integral in (2.8) approaches

$$\lim_{\epsilon \to 0} \oint_{loop} \vec{E} \cdot d\vec{l} \to E^{\parallel}_{above} l - E^{\parallel}_{below} l. \tag{2.9}$$

Therefore the tangential component of the electric field is always continuous across any boundary,

$$E^{\parallel}_{above} = E^{\parallel}_{below}. \tag{2.10}$$

The integrals in (2.4) and (2.8) were evaluated over an infinitesimal region on S. Therefore the boundary conditions on the components of the electric field are only valid near the boundary S.

2.1.2 Uniqueness Theorem

The solutions to (2.3) are general, and what makes them unique are the boundary conditions on the electric field for a given domain. Specifying the value of Φ on a boundary is called a Dirichlet boundary condition, and specifying the normal component of the electric field, $\hat{n} \cdot \vec{\nabla}\Phi$, on a boundary is called a Neumann boundary condition. The uniqueness theorem states [10] that if one finds a solution that satisfies Laplace's equation and the boundary conditions, then it is the unique solution to the problem. To prove the uniqueness theorem, assume that Φ_1 and Φ_2 both satisfy Laplace's equation in some volume V, and they both satisfy the same boundary conditions on the surface S of V. One must show that $\Phi_1 = \Phi_2$.

Let $\vec{F}(\mathbf{r})$ be the function

$$\vec{F}(\mathbf{r}) = (\Phi_1 - \Phi_2)\vec{\nabla}(\Phi_1 - \Phi_2), \tag{2.11}$$

and integrate $\vec{\nabla} \cdot \vec{F}$ over the volume of the domain. Applying Gauss's theorem,

$$\int_V \vec{\nabla} \cdot F d^3\mathbf{r} = \int_S (\Phi_1 - \Phi_2)\hat{n} \cdot \vec{\nabla}(\Phi_1 - \Phi_2) dA. \tag{2.12}$$

Since both Φ_1 and Φ_2 satisfy the same boundary conditions on S, either $\Phi_1 = \Phi_2$ or $\hat{n}\cdot\vec{\nabla}\Phi_1 = \hat{n}\cdot\vec{\nabla}\Phi_2$. In either case the right hand side of (2.12) is zero.

The integrand in (2.12) becomes, $\vec{\nabla} \cdot (fG) = \vec{\nabla}(\Phi_1 - \Phi_2) \cdot \vec{\nabla}(\Phi_1 - \Phi_2) + (\Phi_1 - \Phi_2)\nabla^2(\Phi_1 - \Phi_2)$, where the last term is 0 since Φ_1 and Φ_2 both satisfy Laplace's equation. Therefore (2.12) can be rewritten as,

$$\int_V \left[\vec{\nabla}(\Phi_1 - \Phi_2)\right]^2 d^3\mathbf{r} = 0. \tag{2.13}$$

The only way the integral can be zero is if $\vec{\nabla}(\Phi_1 - \Phi_2) = 0$ for all $\mathbf{r}$, which implies $\Phi_1 - \Phi_2$ must be a constant C independent of $\mathbf{r}$. However, if there is a Dirichlet boundary condition, Φ_1 and Φ_2 would have the same value on that boundary, and the constant C can be set to 0. Thus,

$$\Phi_1 = \Phi_2. \tag{2.14}$$

Therefore any solution which satisfies Laplace's equation, and the Dirichlet and Neumann boundary conditions is the unique solution to the problem.

2.2 Numerical Integration

One can approximate the integral of a function, $f(x)$, by a sum of N trapezoids with width Δx

$$\int f(x)dx \approx \Delta x \sum_{n=1}^{N} \frac{f(x_n) + f(x_n + \Delta x)}{2}. \tag{2.15}$$

As the number of trapezoids, N, tends to infinity the sum in (2.15) approaches the exact value for the area under the curve.

2.3 Numerical Differentiation

Consider a Taylor series expansion of the function $f(x)$ around the point x_0;

$$f(x) = f(x_0) + (x - x_0)\frac{df(x_0)}{dx} + \frac{(x - x_0)^2}{2}\frac{d^2f(x_0)}{dx^2} + O\left((x - x_0)^3\right). \tag{2.16}$$

The value of the function at $x = x_0 + \Delta x$ is

$$f(x_0 + \Delta x) = f(x_0) + \Delta x\frac{df(x_0)}{dx} + \frac{\Delta x^2}{2}\frac{d^2f(x_0)}{dx^2} + O\left(\Delta x^3\right). \tag{2.17}$$

Similarly the value at $x = x_0 - \Delta x$ is

$$f(x_0 - \Delta x) = f(x_0) - \Delta x\frac{df(x_0)}{dx} + \frac{\Delta x^2}{2}\frac{d^2f(x_0)}{dx^2} - O\left(\Delta x^3\right). \tag{2.18}$$

Subtracting (2.18) from (2.17) gives an approximation of the first derivative of $f(x)$ at the point x_0

$$\frac{df(x_0)}{dx} = \frac{f(x_0 + \Delta x) - f(x_0 - \Delta x)}{2\Delta x} - O\left(\Delta x^2\right). \tag{2.19}$$

Adding (2.18) and (2.17) gives an approximation of the second derivative of $f(x)$ at the point x_0

$$\frac{d^2f(x_0)}{dx^2} = \frac{f(x_0 + \Delta x) - 2f(x_0) + f(x_0 - \Delta x)}{\Delta x^2} - O\left(\Delta x^2\right). \tag{2.20}$$

Equations (2.19) and (2.20) can be generalized to approximate the first and second order partial derivatives of $f(x, y)$

$$\frac{\partial f(x_0, y_0)}{\partial x} = \frac{f(x_0 + \Delta x, y_0) - f(x_0 - \Delta x, y_0)}{2\Delta x} - O\left(\Delta x^2\right), \tag{2.21}$$

and

$$\frac{\partial^2 f(x_0, y_0)}{\partial x^2} = \frac{f(x_0 + \Delta x, y_0) - 2f(x_0, y_0) + f(x_0 - \Delta x, y_0)}{\Delta x^2} - O\left(\Delta x^2\right). \tag{2.22}$$

By symmetry, one can fix the coordinate x in equations (2.21) and (2.22) to find the first and second order partial derivatives with respect to the coordinate y

$$\frac{\partial f(x_0, y_0)}{\partial y} = \frac{f(x_0, y_0 + \Delta y,) - f(x_0, y_0 - \Delta y)}{2\Delta y} - O\left(\Delta y^2\right), \tag{2.23}$$

and

$$\frac{\partial^2 f(x_0, y_0)}{\partial y^2} = \frac{f(x_0, y_0 + \Delta y) - 2f(x_0, y_0) + f(x_0, y_0 - \Delta y)}{\Delta y^2} - O\left(\Delta y^2\right). \tag{2.24}$$

It is also useful to know the approximation of a mixed partial derivative. In such cases one needs to apply the first order partial differential operator with respect to y, to equation (2.21), and then approximate. The result is:

$$\begin{aligned} \frac{\partial^2 f(x_0, y_0)}{\partial y \partial x} &= \Big[f(x_0 + \Delta x, y_0 + \Delta y) - f(x_0 - \Delta x, y_0 + \Delta y) \\ &+ f(x_0 - \Delta x, y_0 - \Delta y) - f(x_0 + \Delta x, y_0 - \Delta y)\Big] \Big/ 4\Delta y \Delta x \\ &+ O\left(\Delta x^2\right) + O\left(\Delta y^2\right) \end{aligned} \tag{2.25}$$

2.4 The Discrete Laplace Equation on a Square Lattice in Cartesian Coordinates

Laplace's equation in Cartesian coordinates is,

$$\frac{\partial^2 f(x, y)}{\partial x^2} + \frac{\partial^2 f(x, y)}{\partial y^2} = 0. \tag{2.26}$$

On a square lattice the partial derivatives in (2.26) can be approximated using (2.22) and (2.24). Then after solving for $f(x, y)$ the resulting discrete form of the Laplace equation gives an estimate for the value of the function $f(x, y)$ at every lattice site (x_i, y_i)

$$f(x_i, y_i) = \frac{1}{4}\Big[f(x_i + \Delta x, y_i) + f(x_i - \Delta x, y_i) + f(x_i, y_i + \Delta y) + f(x_i, y_i - \Delta y)\Big] \tag{2.27}$$

where it was assumed the lattice spacing Δx and Δy are equal. The value of $f(x, y)$ at the lattice site (x_i, y_i) is the average of the values of $f(x, y)$ at the nearest neighbour sites. For a square lattice there are four nearest neighbours.

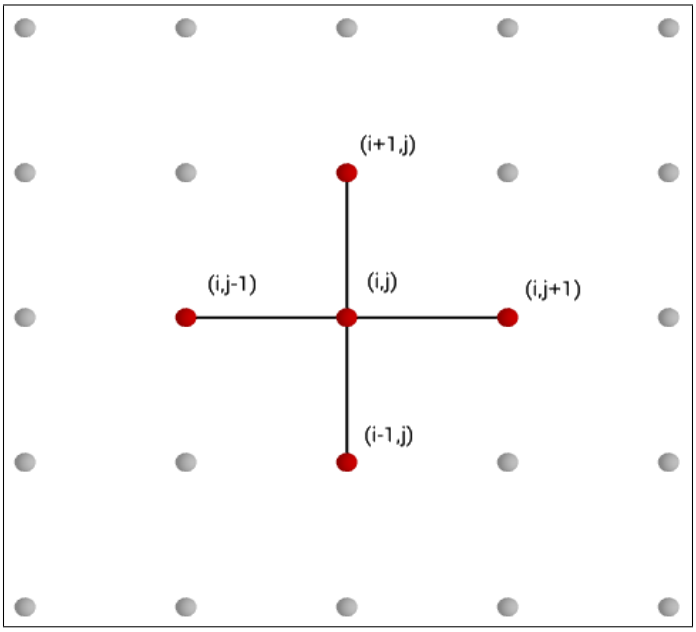

Figure 2.1: This figure illustrates how Laplace's equation is approximated on a square lattice.

2.5 The Discrete Laplace Equation on a General Distribution of Nodes

It will be shown in this section that the discrete form of Laplace's equation for a function, $f(x, y)$, on a general distribution of nodes solution is approximated by

$$f(x_i, y_i) = \frac{\sum_{k=1}^{n} f(\chi_k)\Delta\theta_{kk+1}}{\sum_{k=1}^{n} \Delta\theta_{kk+1}}, \tag{2.28}$$

where χ_k is the position of the nearest neighbour sites relative to the node (x_i, y_i), $\Delta\theta_{kk+1}$ is the angle between the vectors $\chi_k - (x_i, y_i)$ and $\chi_{k-1} - (x_i, y_i)$, and n is the number of nearest neighbours. For a general distribution of nodes, one can define the nearest neighbours relative to a given node as being all other nodes in the distribution which lie within a shell of thickness Δa at a distance a, where a is a constant analogous to the lattice spacing and $\Delta a \propto a$. Then the solution to Laplace's

equation, at a node (x_i, y_i) is the weighted average of the bond angles between adjacent nearest neighbour nodes within the neighbourhood (2.28). The weight factors are the values of the function $f(\chi_k)$ at the nodes in the neighbourhood.

For the square, honeycomb, and triangular lattice the angle between nearest neighbours is constant. For these regular lattices, $\Delta\theta_{kk+1}$ in (2.28) can be removed from the sum. Then the value of the potential at a particular lattice site is the average of the values of the potential at the nearest neighbour sites. Equation (2.28) reduces to

$$f(x_i, y_i) = \frac{\sum_{k=1}^{n} f(\chi_k)}{n} \tag{2.29}$$

which is the general form for the discrete Laplace equation on a regular lattice. Equation (2.27) is a specific instance of (2.28), when the number of nearest neighbours is $n = 4$.

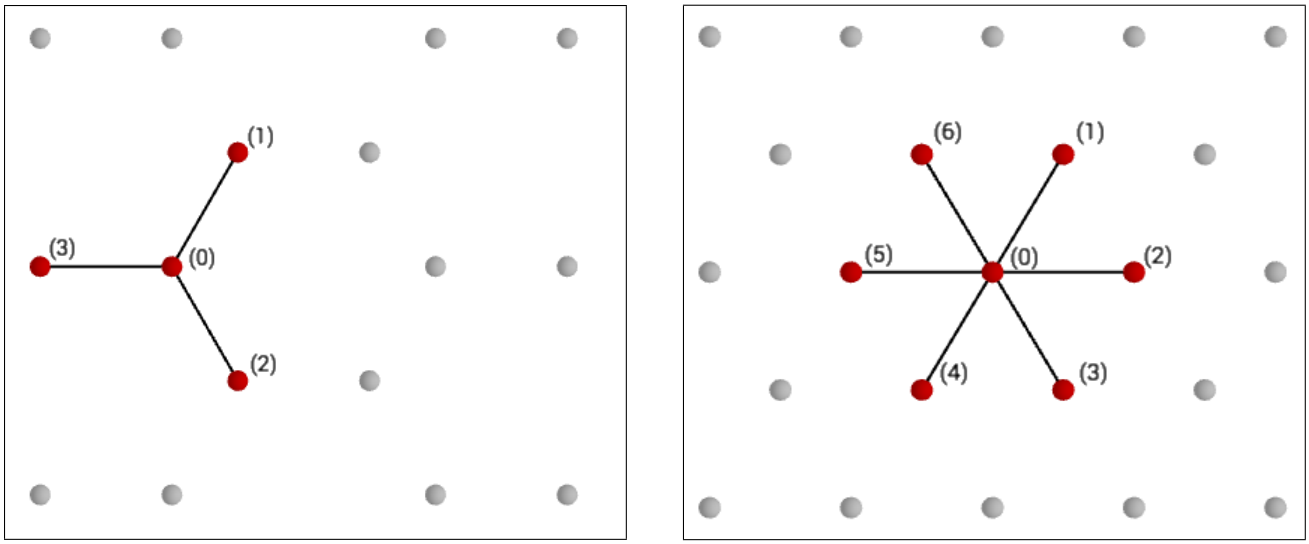

(a) (b)

Figure 2.2: This figure illustrates how Laplace's equation is approximated on (a) honeycomb, and (b) triangular lattice types.

For a random distribution of nodes, the angle between nearest neighbours, and the number of nearest neighbours is no longer constant. The number of nearest neighbours will vary depending on which node the neighbourhood shell Δa is centered on, and the thickness of Δa. A random distribution of nodes with an average neighbourhood that contains 4 nodes is similar to a regular square lattice, as long as the variation from the average number of nearest neighbours is small for

different nodes in the distribution.

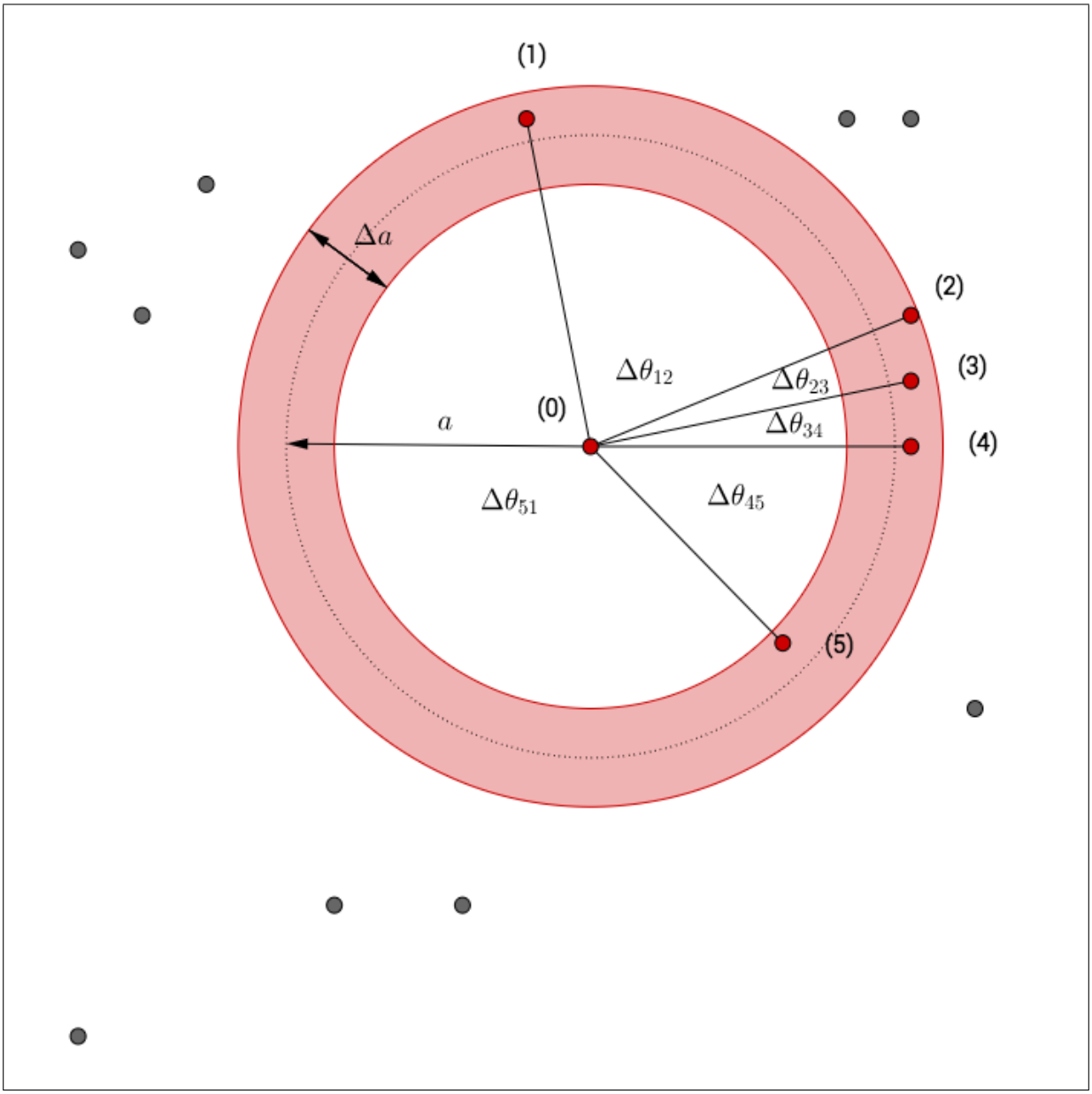

Figure 2.3: This figure illustrates how Laplace's equation is approximated on a random distribution of nodes. The neighbourhood is defined as the shell with thickness Δa, centered on the node (0) (where the potential is calculated). The nearest neighbours to the node (0) are all those points which lie within the shell. The potential at (0) is given by (2.28).

Using (2.28) or (2.29) to find a solution to Laplace's equation can be justified with arguments from complex analysis. Given that $z = x + iy$, if $f(z) = u(x, y) + iv(x, y)$ is analytic, then both u and v must satisfy Laplace's equation. Also, $f(z)$ is a solution since it is a linear combination of u and v. Cauchy's integral formula states that if $f(z)$ is analytic within a closed circular contour c

then

$$\oint_c \frac{f(z)}{z - z_0} dz = 2\pi i f(z_0). \tag{2.30}$$

Then rewrite z in its polar form as $z_0 + a\exp[i\theta]$, and (2.30) becomes

$$\frac{1}{2\pi}\int_0^{2\pi} f\left(z_0 + a\exp[i\theta]\right) d\theta = f(z_0). \tag{2.31}$$

The value of the function at z_0, is determined by the values of the function on the boundary c, or in our case the potential at z_0 is determined by the values of the potential at the nodes within the shell of thickness Δa. Using a circular contour is justifiable if the variation of the radius of the contour is within the thickness of the shell (see discussion below). Noting that $\sum_{k=1}^{n} \Delta\theta_{kk+1} = 2\pi$, the discrete form of (2.31) is $f(z_0) = \sum f(z_k)\Delta\theta_{kk+1} \Big/ \sum \Delta\theta_{kk+1}$, which is the same as (2.28).

The expansion of the function $f(z)$ around the point z_0 is given by (2.17), where $z = z_0 + r\exp[i\theta]$,

$$f(z_0 + r\exp[i\theta]) = f(z_0) + r\exp[i\theta]\frac{df(z_0)}{dz} + O\left(r\exp[i\theta]\right)^2. \tag{2.32}$$

Equation (2.32) is the approximation of the potential at a node within the shell. Substituting $r = a + \frac{\Delta a}{2}$ into (2.32) gives an approximation of the potential if the node was moved to the outer ring of the shell,

$$f\left(z_0 + \left[a + \frac{\Delta a}{2}\right]\exp[i\theta]\right) = f(z_0) + \left[a + \frac{\Delta a}{2}\right]\exp[i\theta]\frac{df(z_0)}{dz} + O\left(\left[a + \frac{\Delta a}{2}\right]\exp[i\theta]\right)^2. \tag{2.33}$$

Substituting $r = a - \frac{\Delta a}{2}$ into (2.32) gives an approximation of the potential if the node was moved to the inner ring of the shell,

$$f\left(z_0 + \left[a - \frac{\Delta a}{2}\right]\exp[i\theta]\right) = f(z_0) + \left[a - \frac{\Delta a}{2}\right]\exp[i\theta]\frac{df(z_0)}{dz} + O\left(\left[a - \frac{\Delta a}{2}\right]\exp[i\theta]\right)^2. \tag{2.34}$$

Subtracting (2.34) from (2.33) gives,

$$f\left(z_0 + \left[a + \frac{\Delta a}{2}\right]\exp[i\theta]\right) - f\left(z_0 + \left[a - \frac{\Delta a}{2}\right]\exp[i\theta]\right) = \Delta a\exp[i\theta]\frac{df(z_0)}{dz} \tag{2.35}$$

where error terms have been neglected since it is assumed that a and $\frac{\Delta a}{2}$ are proportional to the inverse of the total number of nodes, $1/N << 1$. Equation (2.35) says that for a constant θ the potential difference between the outer and inner ring of the neighbourhood shell is on the order of Δa. For a large distribution of nodes the shell's thickness can be ignored, then any circular contour c with a radius that is inside the shell's boundary can be used to evaluate (2.30) with a maximum uncertainty equal to,

$$\int_0^{2\pi} f_+ d\theta - \int_0^{2\pi} f_- d\theta = \Delta a \int_0^{2\pi} \exp[i\theta] \frac{df(z_0)}{dz} d\theta \tag{2.36}$$

where f_+ is shorthand for (2.33) and f_- for (2.34). In this way the variation of the radius of the contour can be neglected within the shell, and (2.31) or its numerical approximation (2.28) can be used to find a solution to Laplace's equation with an uncertainty on the order of Δa. Neglecting terms on the order of Δa and using (2.28) to find a solution to Laplace's equation does not affect the dielectric breakdown results (see more discussion in section 3.2).

2.6 The Discrete Laplace Equation on a Square Lattice in Transformed Coordinates (η, ζ)

In this thesis, a method will be developed to find the electrical resistance of any solid of revolution, as long as the generating curve is known. The particular solids studied in this thesis are truncated conical, ellipsoidal, and hyperboloidal resistors, as shown in Fig. 1.2. They are in cylindrical coordinates (s, θ, z), with their axis of symmetry aligned with the z-axis. In general, the generating curve for any solid of revolution, in cylindrical coordinates, can be written as

$$\left(\frac{s}{b}\right)^2 - \left(\frac{f(z)}{h}\right)^2 = 0, \tag{2.37}$$

and the solid is the volume enclosed from rotating the curve around the z-axis in the θ-direction. The function $f(z)$ for a truncated ellipsoidal resistor is $\sqrt{h^2 - z^2}$, because after substitution into (2.37) the equation of an ellipse is recovered. Similarly $f(z) = \sqrt{h^2 + z^2}$ for a truncated hyperboloidal resistor, and $f(z) = z$ for a truncated conical resistor. The value of h depends on the height L and

the ratio a/b of the resistors (Fig. 1.2). For the truncated conical resistor, $h = L/(1-a/b)$, and for the truncated ellipsoidal and hyperboloidal resistors, $h = L/\sqrt{1-(a/b)^2}$, and $h = L/\sqrt{1+(a/b)^2}$, respectively.

As mentioned in section 1.1, the problem of finding the resistance of a solid reduces to solving Laplace's equation for the electric potential everywhere inside. It is assumed that the electric potential is independent of the azimuthal angle θ, because the resistors have rotational symmetry around the $\hat{z}$-axis. Thus the problem is effectively two dimensional with only the radius, s, and height, z, being important to the calculation. The appropriate Laplace equation in cylindrical coordinates for electric potential $\Phi(s,z)$ is

$$\frac{\partial^2\Phi}{\partial s^2} + \frac{1}{s}\frac{\partial\Phi}{\partial s} + \frac{\partial^2\Phi}{\partial z^2} = 0. \tag{2.38}$$

The boundary conditions are provided by the physical boundaries of the resistors. There are Dirichlet boundary conditions on the cross sectional surfaces with radius a and b. On these surfaces the potential is constant $\frac{d\Phi}{dz}\Big|_a = 0$ and $\frac{d\Phi}{dz}\Big|_b = 0$. There is also a Neumann boundary condition at the side of the resistors. The side of the resistors are implicitly defined by (2.37). The electric field must be parallel to the side of the resistors at $s = \frac{b}{h}f(z)$. The Neumann boundary condition can be stated as,

$$\vec{\nabla}\Phi \cdot \hat{n}\Big|_{s=\frac{b}{h}f(z)} = 0 \tag{2.39}$$

where $\hat{n}$ is the normal vector to the sides of the resistor, and $\vec{\nabla}\Phi$ is the electric field. Solving the system of equations (2.38) and (2.39) numerically requires approximating them by difference equations, as mentioned in section 2.3 and section 2.4. The ranges of s, and z can be discretized on a rectangular lattice, and the electric potential Φ can be computed for each node (s_j, z_i). However, since the sides of the resistor are not parallel to the rectangular boundaries of the lattice, the curve which defines the sides of the resistor will not intersect the nodes of the lattice. Therefore, it is advantageous to transform the coordinates (s,z) to new coordinates (η,ζ), such that in these new coordinates the sides of the resistor are constant coordinate surfaces, parallel to the rectangular lattice (η_j, ζ_i).

The transformation to coordinates (η, ζ) is motivated from (2.37), and given by,

$$\begin{aligned} \eta &= \frac{1}{2}\left(\frac{s}{f(z)}\right)^2 \\ \zeta &= \frac{z}{k} \end{aligned} \tag{2.40}$$

where the variable k is a constant parameter, with a value of L/η_0, that ensures the lattice spacing is the same in the η and ζ directions. We chose to include the power of two in the η coordinate, because this ensures there are no coefficients proportional to $1/\eta$ in the transformed Laplace equation (2.41). Terms proportional to $1/\eta$ would introduce a singularity at the central axis ($s = 0$) of the resistors. In the transformed coordinates, the boundaries of the resistor are given by constant values, and the range of η and ζ can be discretized on a square lattice. The transformed Laplace equation is

$$2\eta\left(k^2 + 2\eta\dot{f}^2\right)\Phi_{\eta\eta} + 2\left(k^2 - \eta\ddot{f}f + 3\eta\dot{f}^2\right)\Phi_\eta + f^2\Phi_{\zeta\zeta} - 4\eta\dot{f}f\Phi_{\eta\zeta} = 0 \tag{2.41}$$

where the function f is the generating curve for the side of the resistor, and $\dot{f}$ denotes $\frac{df(\zeta k)}{d\zeta}$. On the sides of the resistor, boundary condition (2.39) becomes

$$\left(k^2 + 2\eta_0\dot{f}^2\right)\Phi_\eta - \dot{f}f\Phi_\zeta = 0 \tag{2.42}$$

where the constant η_0 is the value η has on the boundary of the resistor, and it is equal to $\frac{1}{2}\left(\frac{b}{h}\right)^2$. For the purposes of numerical calculations, the origin of the resistor ($\eta = 0$) will be a boundary of the square lattice; setting $\eta = 0$ in (2.41),

$$2k^2\Phi_\eta + f^2\Phi_{\zeta\zeta} = 0. \tag{2.43}$$

The discrete version of equations (2.41) - (2.43) can be obtained by approximating the partial derivatives of Φ (see Eq. 2.21 - 2.25), and the ranges of η and ζ on a square lattice. The discrete

form of the transformed Laplace equation (2.41) is

$$A_{i,j}\left(\Phi_{i,j+1}-2\Phi_{i,j}+\Phi_{i,j-1}\right)+B_{i,j}\left(\Phi_{i,j+1}-\Phi_{i,j-1}\right)+C_{i,j}\left(\Phi_{i+1,j}-2\Phi_{i,j}+\Phi_{i-1,j}\right)+D_{i,j}M_{i,j}=0$$

which, after solving for $\Phi_{i,j}$, simplifies to

$$\Phi_{i,j}=\frac{1}{2}\left(A_{i,j}+C_{i,j}\right)^{-1}\Big(\Phi_{i,j+1}\left[A_{i,j}+B_{i,j}\right]+\Phi_{i,j-1}\left[A_{i,j}-B_{i,j}\right]+C_{i,j}\left[\Phi_{i+1,j}+\Phi_{i-1,j}\right]+D_{i,j}M_{i,j}\Big). \tag{2.44}$$

The coefficients A, B, C, D in (2.44) are the discrete forms of the coefficients in (2.41) divided by the appropriate lattice spacing term

$$\begin{aligned}
A_{i,j} &= \frac{2\eta_j\left(k^2+2\eta_j\dot{f}_i^2\right)}{\Delta\eta^2}\\
B_{i,j} &= \frac{2\left(k^2-\eta_j\ddot{f}_i f_i+3\eta_j\dot{f}_i^2\right)}{2\Delta\eta}\\
C_{i,j} &= \frac{f_i^2}{\Delta\zeta^2}\\
D_{i,j} &= \frac{-4\eta_j\dot{f}_i f_i}{4\Delta\eta\Delta\zeta}
\end{aligned}$$

The term $M_{i,j}$ is the approximation of the mixed partial derivative of Φ (see Eq. 2.25). It is implied that the index i and j label the rows and columns of a matrix, of which each element represents a lattice site. The origin of the resistor, where $\eta = 0$, is represented as all of the lattice sites belonging to the first column ($j = 1$) of the matrix. Similarly, the side of the resistor,where $\eta = \eta_0$, is represented as all of the lattice sites belonging to the last column ($j = N$) of the matrix. Finally, the two electrode surfaces are given by the first and last rows ($i = 1, i = N$) of the matrix.

The ranges of i and j are only defined for integer values on the interval $[1, N]$. No approximation of a partial derivative at the boundaries can contain terms which would call for an index outside the range of i and j; either $N+1$ or 0. As an example, consider the approximation of Φ_η at $j = N$: $\Phi_{i,N} = \left(\Phi_{i,N+1}-\Phi_{i,N-1}\right)\Big/2\Delta\eta + O\left(\Delta\eta^2\right)$. This is a second order approximation to the derivative, because the error is proportional to $(\Delta\eta)^2$, however it contains the term $\Phi_{i,N+1}$ which is not allowed

on the boundary. The solution is to approximate the derivative using a backwards first order approximation (i.e. with an error proportional to $\Delta\eta$). It can be shown, using (2.18), that the first order approximation to the derivative on the side boundary is $\Phi_{i,N} = (\Phi_{i,N} - \Phi_{i,N-1}) \Big/ \Delta\eta + O(\Delta\eta)$. Similarly, at the origin, the approximation to the derivative cannot contain the term $\Phi_{i,0}$. It can be shown using (2.17), the first order approximation to the derivative at the origin boundary is, $\Phi_{i,1} = (\Phi_{i,2} - \Phi_{i,1}) \Big/ \Delta\eta + O(\Delta\eta)$.

One can use the first order approximations of Φ_η to find the discrete form of the boundary conditions. The discrete form of the boundary condition on the side (2.42) is

$$\Phi_{i,N} = \Phi_{i,N-1} + \frac{\dot{f}_i f_i}{k^2 + 2\eta_0 \dot{f}_i^2} \frac{\Delta\eta}{2\Delta\zeta} (\Phi_{i+1,N} - \Phi_{i-1,N}) \tag{2.45}$$

and at the origin (2.43) of the lattice

$$\Phi_{i,1} = \frac{1}{2} (B_{i,1} + C_{i,1})^{-1} \Big(2B_{i,1}\Phi_{i,2} + C_{i,1} [\Phi_{i+1,1} + \Phi_{i+1,1}] \Big). \tag{2.46}$$

The set of linear equations (2.44) - (2.46) can be solved numerically using Gauss-Seidel successive over-relaxation (section 2.7) to obtain an approximate value of the electric potential, Φ, at every lattice site. Then the resistance is given by $R = \Delta\Phi/I$, where I is the total current, and $\Delta\Phi$ is the potential difference between the two electrodes. The total current is found by integrating the normal component of the current density, $\vec{J} = -\sigma\vec{\nabla}\Phi$, through any circular cross section perpendicular to the z-axis:

$$I = -\sigma \int\int \nabla_z \Phi s ds d\theta = -2\pi\sigma \int \frac{\partial\Phi}{\partial z} s ds. \tag{2.47}$$

The derivative $\frac{\partial\Phi}{\partial z}$ in (2.47) is evaluated at a particular height z in the resistor, and is therefore a function of s only. One can transform (2.47) to (η, ζ) coordinates using the reverse transformation of (2.40)

$$I = -2\pi\sigma \int_0^{\eta_0} \left(-2\eta \dot{f} \Phi_\eta + \frac{f^2}{k} \Phi_\zeta \right) d\eta. \tag{2.48}$$

The total current can be evaluated numerically using the method discussed in section 2.2. It can be shown that $f(\zeta k) \sim L$ and therefore $I \sim \sigma L$, by substituting the definition of h and k in to f.

2.7 Gauss-Seidel Successive Over-Relaxation

Given the discrete form of Laplace's equation, and initial values for the potential on a square lattice, relaxation is an iterative method that successively converges to an approximate solution. During each iteration a value of the potential, Φ, is assigned for every lattice site, according to the discrete equation for those lattice sites. Assuming that one is iterating through lattice sites with increasing i and j, the successive over relaxation method takes a linear combination of potential values from subsequent iterations in order to converge to a solution

$$\Phi_{i,j}^{n+1} \rightarrow (1-w)\Phi_{i,j}^{n} + w\Phi_{i,j}^{n+1} \tag{2.49}$$

where n is the iteration number, and w is a relaxation parameter. For quick convergence, $1 < w < 2$, with an optimal value for $w = 2 - \pi\Delta$ [11] on a square lattice, where Δ is the lattice spacing. After each iteration, the values of the potential at all the lattice sites from the previous iteration are subtracted from the new values. Over multiple iterations, the maximum difference in the values of the potential between successive iterations becomes smaller. When the maximum difference in potential values approaches a predefined constant tolerance value, usually when $\max(|\Phi^{n+1} - \Phi^{n}|) \leq 10^{-12}$, the iterations stop.

2.8 Dielectric Breakdown Model Algorithm

Dielectric breakdown simulation proceeds iteratively on a lattice. In this project a 2D square, honeycomb, and triangular lattice were studied, as well as a random distribution of nodes. The nodes of the lattice represent the possible sites which the electron can occupy (i.e. atoms or molecules), and the connective lines between nearest neighbour sites represent the bonds between atoms or molecules (see Fig. 2.1, 2.2, and 2.3). Initially an electric field is created by the potential difference between the electrode at the center of the lattice, and the other electrode is modelled as a circle of constant potential far away. The potential at the electrode at the center of the lattice is 0V, and the potential is 1V everywhere on the circumference of the circle far away. Using the methods discussed in this chapter, the electric potential is solved for every node on the lattice, subject to

the potential boundary conditions. Electrons freely move to lattice sites where the potential is 0V. Electrons randomly jump to neighbouring lattice sites with a probability proportional to the strength of the local electric field (2.50). Once an electron occupies a neighbouring site, the potential for that site is set to 0V. Each addition of an electron changes the electric field configuration, and the potential must be re-calculated before another perimeter site is chosen to be occupied.

The probability that an electron at lattice site, (i, j), will occupy a neighboring site, (i', j'), is proportional to the potential difference across the bond raised to some exponent, η,

$$p(i, j \to i', j') = \frac{(\Phi_{i',j'})^\eta}{\sum(\Phi_{i',j'})^\eta}. \tag{2.50}$$

The potential on the lattice sites that an electron occupies is always 0V, $\Phi_{i,j} = 0$, and that is why the term does not appear in (2.50). The summation in (2.50) goes over all nearest neighbour sites, (i', j'), relative to the cluster. To decide which neighbouring site of the cluster will be occupied, one first randomly selects a neighbouring site, and assigns an occupation probability to that site according to (2.50). Next a random number between 0 and 1 is generated. If the random number is less than or equal to the probability of occupation for that site, then that site will be occupied (i.e. the potential will be set to 0V), otherwise another neighbouring site is randomly selected, and the choosing process continues. Therefore, the larger the occupation probability is for a perimeter site, the more likely it is that the random number between 0 and 1 will be less than that probability, and the more likely it is the electron will occupy that site.

It is clear that the role of the exponent, η, is to control how much of an influence the electric field has on the probability of a neighboring site being occupied. In the extreme case of $\eta = 0$, every neighboring site has equal chance of being occupied, and the overall breakdown structure will resemble a random walk in 2D. Alternatively, as η is increased to larger positive values, it becomes increasingly likely that only those bonds which have a large potential difference will facilitate electron conduction, and allow nearest neighbour sites to be occupied. The tips of growing clusters which are closer to the boundary of the lattice will experience a larger local electric field. As a result of (2.50), the tips of the cluster are more likely to continue to grow. Perimeter sites of the cluster which are surrounded by growing branches are less likely to facilitate growth, as the local

electric field is negligible due to the potential being 0V on the surrounding branches. These two modes of cluster growth are known as the "tip effect" and "Faraday screening"[6].

Solving for the electric field during each iteration has a time complexity on the order of $O(N^3)$. To reduce computation time one can assign larger probabilities to the growth of tips with respect to side branching [12]. This assumes the distribution of the electric field without explicitly solving it. This simplification, however, assigns the same growth probability to a tip inside a Faraday screen and a free tip, because there is no electric field to distinguish the two tips. The resulting fractal dimension of the clusters is close to the embedding dimension, and they do not resemble experimental discharges [6].

2.9 Fractal Dimension

This section references the arguments found in chapters 2-4 in the book "Fractal Growth Phenomena"[13], by Tamas Vicsek.

Fractals are patterns which exhibit self-similarity over multiple length scales. Mathematical fractals are created by the repeated addition of a pre-determined pattern. Mathematical fractals are infinitely divisible, and self-similar over an infinite range of length scales. Examples of mathematical fractals include the Sierpinski carpet, the Koch curve, and the Mandelbrot set. A subset of a mathematical fractal can be repeatedly magnified with no change to the appearance of the pattern. The dielectric breakdown model produces clusters which are statistical fractals, by the repeated addition of a randomly selected lattice site. In contrast, statistical fractals display self-similarity over a finite range of length scales. Unlike mathematical fractals, statistical fractals do not have the property of similar appearance on multiple length scales, however the number density of sites belonging to the fractal will be scale invariant. The fractal dimension is defined as the exponent D in the scaling relationship between the number of sites $N(L)$, which belong to the fractal in some circle of radius L, and L

$$N(L) \sim L^D \tag{2.51}$$

For a two dimensional lattice, the number of sites $N(L)$ will be proportional to the area of the

lattice (L^2) and the dimension is $D = 2$. For a fractal, the exponent D is a non-integer value, because the cluster occupies a fraction of the lattice sites. The distribution of mass in the cluster can give rise to a spectrum of fractal dimensions (see subsection 2.9.1).

Alternatively, by covering the cluster with a grid of cell size l, the total number of cells required to completely cover the fractal, $N(l)$, scales with l as

$$N(l) \sim l^{-D} \tag{2.52}$$

For growing fractals, l is constant and L is increasing, then the fractal dimension is found with (2.51). While for fractals generated by subsequent divisions, L is constant and the size of the unit being added, l, is decreasing, then the fractal dimension is found with (2.52). Both physical cases can be accounted for by introducing a dimensionless quantity, $\epsilon = l/L$, which is the size of the normalized units covering the fractal. The number of dimensionless units needed to completely cover the fractal, $N(\epsilon)$, scales with ϵ as

$$N(\epsilon) \sim \epsilon^{-D} \tag{2.53}$$

A variation on (2.51) is to calculate the radius of gyration of the cluster at different stages during its growth, using the formula [14],

$$R_g^2 = \frac{1}{2N^2} \sum_{i,j=1}^{N} |r_i - r_j|^2 \tag{2.54}$$

where r_i and r_j are the position vectors of the i^{th} and j^{th} lattice site, or particle, belonging to the structure and N is the total number of particles. This is done for growing fractals, where particles of constant size are subsequently added to the structure. It is then assumed that the radius of gyration obeys the relation

$$R_g^2 \sim N^{2/D} \tag{2.55}$$

where D is the fractal dimension. Equation (2.55) is analogous to (2.51), only the reference to size has shifted from L to R_g. In fact, rearranging (2.55) gives, $N \sim R_g^D$. Finite fractals will obey any of

the above scaling laws within a range of length scales. Typically data is displayed on a log-log plot of length scale (L, l, R_g, ϵ) versus N, and the linear portion of the data is where the fractal obeys a scaling law. The slope of the linear portion is related to the fractal dimension. In this thesis fractals were grown on a $2D$ lattice with spacing a. Scaling law behaviour was found when, $a \ll l \ll L$, where l is the size of the cells of a grid which covers the fractal. In terms of the normalized unit ϵ, scaling law behaviour was found when $a/L \ll \epsilon \ll 1$.

2.9.1 Multifractality - Generalized Dimension and Singularity Spectra

In the dielectric breakdown model, the growth of the cluster is determined by the spatial distribution of a scalar electric potential. At the end of growth, every lattice site which belongs to the fractal has a potential of 0V, and at a boundary far from the fractal there is a constant potential of 1V. Since the electric field is the gradient of the potential, near the tips of the branches on the fractal the electric field will be very large (singular). Thus, fractals are a result of a physical process which leads to a spatial distribution of some quantity which contains many singularities. Alternatively, a random walk evenly distributes mass over space with no singularities, and as a result is not a fractal. Moreover, tips at different sites on the fractal may have different local mass distributions (i.e the number of sites which belong to the fractal within a neighbourhood) which will affect the singularity strength of that site. Multifractals have a mass distribution that is made from many sets of singularities with different strengths.

In order to study the multifractality of a mass distribution, a grid with length L and cell size l is placed over the fractal. The probability, p_i is calculated as the number of lattice sites which belong to the fractal within the i^{th} box of the grid, with $\sum_i p_i = 1$. Using the dimensionless unit $\epsilon = l/L$, the scaling of quantities related to p_i can be studied as $\epsilon \to 0$. For uniform mass distributions the probability in each box is the same, so $p \sim \epsilon^d$, where d is the Euclidean dimension. In the general case of multifractals it is assumed [13]

$$p(\epsilon) \sim \epsilon^{\alpha} \tag{2.56}$$

where α is the strength of the local singularity, and can have a different value depending on the position in the fractal. Many sites belonging to the fractal may have the same value of α. The

number of sites that have the same value of α scales with ϵ as

$$N_\alpha(\epsilon) \sim \epsilon^{-f(\alpha)} \tag{2.57}$$

where $f(\alpha)$ is the fractal dimension of the subset of lattice sites characterized by the exponent α. The function $f(\alpha)$ is a concave function with its maximum equal to the fractal dimension D, and the spread of α values provides a measure of multifractality. Very broad $f(\alpha)$ spectra correspond to high multifractality, whereas limited spectra correspond to uniform distribution of mass (low multifractality). Another interpretation of $f(\alpha)$ is to think of it as a measure of the likelihood that an exponent α will be found in the cluster [9].

The function $f(\alpha)$ can be calculated using the quantity

$$\chi_q(\epsilon) \equiv \sum_i p_i^q \tag{2.58}$$

which is determined directly from experimental data. The exponent q can take any real value. The value of q either magnifies dense regions or magnifies rare regions of the mass distribution. For $q = 0$, (2.58) gives, $\chi_0(\epsilon) = \sum_{i=1}^{N(\epsilon)} 1 = N(\epsilon)$, where $N(\epsilon)$ is the number of boxes of size ϵ needed to completely cover the fractal. Using (2.53) one finds that $\chi_0(\epsilon) \sim \epsilon^{-D}$, where D is the fractal dimension. When the exponent q is large and positive, the sum in (2.58) is sensitive to regions of the fractal in which p_i is large (denser regions). When the exponent q is large and negative, the sum in (2.58) is sensitive to regions of the fractal in which p_i is small (rarer regions). The sum in (2.58) scales with ϵ as

$$\chi_q(\epsilon) \sim \epsilon^{(q-1)D_q} \tag{2.59}$$

where D_q is generalized dimension of order q, and it is clear that $D_0 = D$. For multifractals the distribution of D_q's is a function of q. For monofractals all D_q's are equal to D and there is no q dependence on the distribution. For a given value of q there will be a subset of boxes which dominant the sum in (2.58). The number of dominant boxes, $N_q(\epsilon)$, scales with ϵ as

$$N_q(\epsilon) \sim \epsilon^{-f_q} \tag{2.60}$$

where $f_q = f(\alpha_q)$. Each dominant box will also have the same probability $p_i = p_q$, and singularity strength, α_q, defined by

$$p_q \sim \epsilon^{\alpha_q} \tag{2.61}$$

Therefore the sum in (2.58) can be approximated by

$$\chi_q(\epsilon) \approx N_q(\epsilon) p_q^q \tag{2.62}$$

since the number of boxes with probability p_q will dominate the sum. Now substituting (2.59), (2.60), and (2.61) into (2.62), one gets

$$(q-1)D_q = q\alpha_q - f_q \tag{2.63}$$

Typically the generalized dimension spectrum is determined from experimental data by

$$D_q = \lim_{\epsilon \to 0} \frac{1}{q-1} \frac{\ln \sum_i p_i^q}{\ln \epsilon}, \tag{2.64}$$

which is a restatement of (2.59). The singularity strength α_q is calculated through the relation

$$\alpha_q = \frac{d}{dq}[(q-1)D_q] \tag{2.65}$$

Then the $f(\alpha)$ spectrum is numerically determined using (2.64), (2.65), and (2.63). Equation (2.65) follows from expressing the sum in (2.58) as an integral over α. Instead of summing over individual boxes, one counts the number of boxes that have the same value of α and multiplies by the probability in the boxes, p^q, to get $N_\alpha(\epsilon)p(\epsilon)^q$. Then integrating over α gives an approximation of (2.58). Using (2.56) and (2.57)

$$\chi_q(\epsilon) \sim \int \epsilon^{q\alpha' - f(\alpha')} d\alpha' \tag{2.66}$$

When $\epsilon << 1$ the integral will be dominated by an α which minimizes the exponent,

$$\frac{d}{d\alpha}\left[q\alpha - f(\alpha)\right]_{\alpha=\alpha_q} = 0 \rightarrow \frac{df(\alpha_q)}{d\alpha} = q \tag{2.67}$$

Thus, (2.65) follows from taking the derivative of (2.63) with respect to q, and applying the condition in (2.67) with $f_q = f(\alpha_q)$. When $q = 0$ in (2.67) $f(\alpha)$ has a maximum value.

Chapter 3

Results

3.1 Electrical Resistance of Solids Results

The resistance of the truncated conical, ellipsoidal, and hyperboloidal resistors were calculated on a square lattice in the transformed coordinates, with spacing $\Delta\eta = \Delta\zeta = \eta_0/N$, where N is the dimension of the matrix which stores the values of the potential at each lattice site. The resistance was calculated for the matrix dimension, N, ranging from 100 to 3200. It was assumed that the potential difference between electrodes was equal to one (i.e. $\Delta\Phi = 1$), but the solution scales linearly with $\Delta\Phi$. It was also assumed that $L/b = 1$ for all calculations, but the total resistance is inversely proportional to the linear size, L, of the resistor. The total current, $I(N)$ was calculated, using the discrete form of (2.48), at all values of ζ, where ζ is proportional to the coordinate z. In addition, the resistance was calculated for different values of a/b, ranging from 0.1 to 0.9, and fit to the curve, $I\left(\frac{a}{b}\right) = A + B\left(\frac{a}{b}\right) + C\left(\frac{a}{b}\right)^2 + D\left(\frac{a}{b}\right)^3 + E\left(\frac{a}{b}\right)^4$ (Fig. 3.1). This particular fit is motivated from work done by R. S. Timsit [4], in which the expression for the spreading resistance in a constricted cylinder is expanded in a power series of b/a. In their work $b/a < 1$, in our work we expand the current in a power series for $a/b < 1$. The numerical results for the total current in the truncated conical, ellipsoidal, and hyperboloidal resistors are

$$\begin{aligned}
I_{cone} &= \frac{L}{\rho}\left[0.0002 + 2.2822\left(\frac{a}{b}\right) + 1.3714\left(\frac{a}{b}\right)^2 - 0.13762\left(\frac{a}{b}\right)^3 - 0.37488\left(\frac{a}{b}\right)^4\right], \\
I_{ellipsoid} &= \frac{L}{\rho}\left[0.0050 + 3.9459\left(\frac{a}{b}\right) - 1.5609\left(\frac{a}{b}\right)^2 + 1.9725\left(\frac{a}{b}\right)^3 - 1.2246\left(\frac{a}{b}\right)^4\right], \\
I_{hyperboloid} &= \frac{L}{\rho}\left[-0.0007 + 1.2856\left(\frac{a}{b}\right) + 1.0672\left(\frac{a}{b}\right)^2 + 2.2861\left(\frac{a}{b}\right)^3 - 1.4957\left(\frac{a}{b}\right)^4\right]. \quad (3.1)
\end{aligned}$$

The coefficients in (3.1) are dependent on the values of L and b. For a relationship other than $L/b = 1$, the coefficients must be recalculated. A contour plot of the numerically calculated potential shows a solution to Laplace's equation which satisfies the boundary conditions (see Fig. 3.2). It is clear that the electric field, and therefore the current flow, is parallel to the sides of the resistor, and the potential is constant on the cross-sectional surfaces defined by radii a and b. The ratio, a/b, quantifies the deviation of the resistor from a cylindrical resistor. When $a/b = 1$, in all cases the resistance of a cylindrical resistor is recovered, and the contour plot of the numerically calculated potential matches that of the potential distribution for a cylindrical resistor (see Fig. 3.2). The error of the calculation increases with $a/b << 1$ for a fixed matrix dimension, N (see Fig. 3.3). As the surface area of the cross section defined by radius a decreases, the current density across the surface must increase, causing the strength of the local electric field to also increase. Thus a finer mesh is needed in order to resolve the large derivative of the electric potential near the surface of the smaller electrode. The results in this thesis agree with the results given by [3]; when, $a/b = 0.5$ the resistance of the truncated conical resistor is $(0.692 \pm 0.1\%)\,\frac{\rho}{L}$, and the value obtained in this thesis was $(0.6928 \pm 0.08\%)\,\frac{\rho}{L}$.

Ideally the total current should be independent of the value of ζ (i.e. the total current through one electrode should be the same as the total current through the second electrode), however in practice one finds numerical variation in the total current from the average value when calculated at different values of ζ. The error of the average total current is proportional to the maximum difference in the total current values, $\delta I(N) = \frac{1}{2}[I_{max}(N,\zeta) - I_{min}(N,\zeta)]\Big/ I(N)$, where it is assumed, by definition, that $I(N) \equiv I_{avg}(N) = \frac{1}{N}\sum_{i=1}^{N} I(N,\zeta_i)$. It was shown that the error in the average total current can be fit to the equation, $\delta I(N) = A + B/N$. It can be seen in Fig. 3.4 that as the dimension of the matrix increases the error of the calculation decreases as $1/N$. The error in the resistance was then estimated using error propagation rules on the relation, $R = \Delta\Phi/I$ giving $\delta R(N) = \Delta\Phi\left[\delta I(N)\Big/ I(N)^2\right]$.

The numerically calculated resistance is always greater than the textbook resistance, due to a spreading resistance term, caused by the bending of electric field lines [4]. The electric field lines bend to satisfy the boundary conditions of the resistor, and do so in spite of the fact that there is no free charge or significant magnetic field. Thus, the divergence and curl of the electric field are equal

to zero $\left(\vec{\nabla} \cdot \vec{E} = 0, \vec{\nabla} \times \vec{E} = 0\right)$ and not responsible for the bending of the electric field lines. It was shown by J.D. Romano and R.H. Price [5] that nine components are needed to describe the gradient of a general vector field in three dimensions. The divergence and curl of a field only specify four components of the gradient $\vec{\nabla}\vec{E}$. The remaining five components are accounted for by a derivative operation called shear, found in (1.3). The shear of the electric field, $S\left(\vec{E}\right)$, is responsible for the bending of the electric field lines in an electrostatic problem with no free charge. It describes the rate at which a cylindrical element of current density deforms in the resistor. The deformation is due to the constricting of the electric field within the boundaries of the resistor.

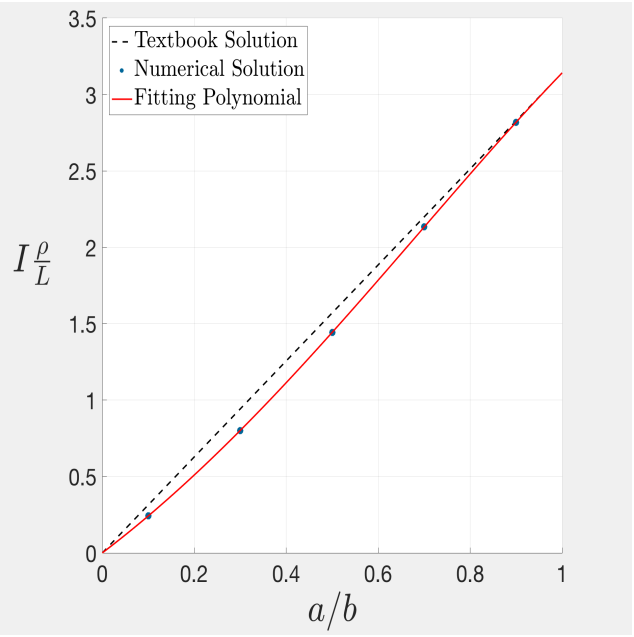

(a) Total current in a truncated conical resistor

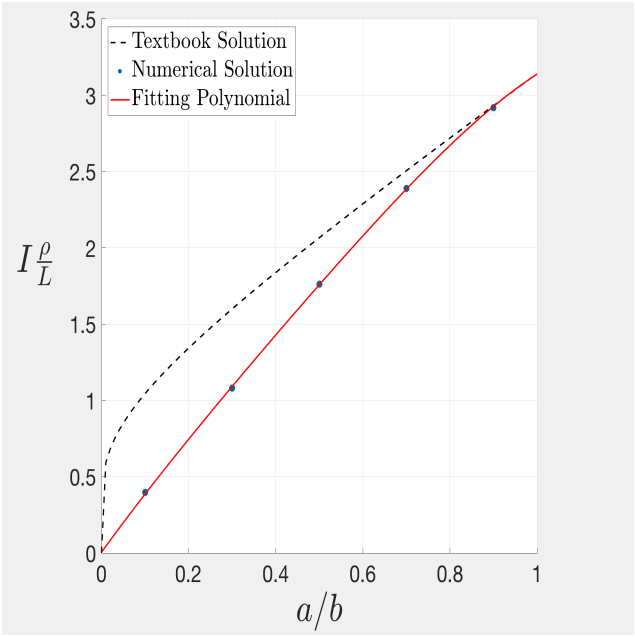

(b) Total current in a truncated ellipsoidal resistor

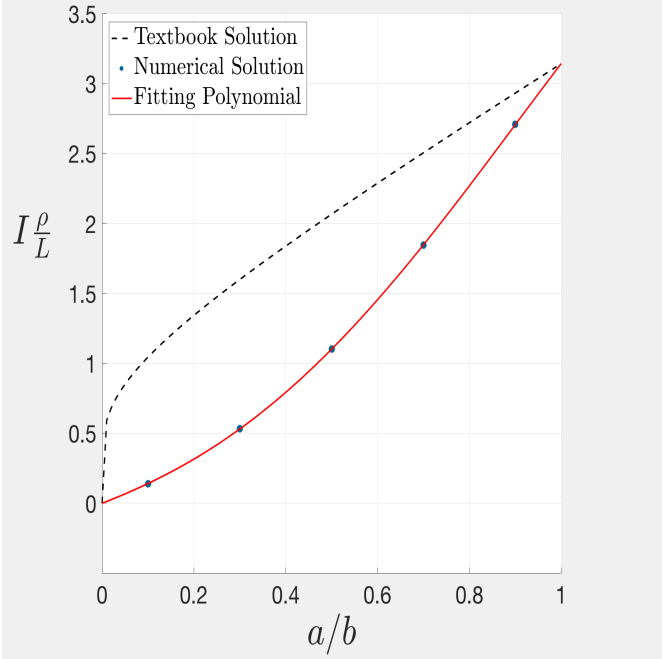

(c) Total current in a truncated hyperboloidal resistor

Figure 3.1: It was assumed that $\Delta\Phi = 1$, and $L/b = 1$. The textbook solution can be determined by dividing the solid resistor into infinitesimal cylindrical elements with resistance, $dR = \rho dz/A(z)$, and integrating over the range of z (see sec. 1.1). Then the total current is $1/R$. The fit equations are given by (3.1). For each resistor, the value of the current converges to the current in a cylinder when $a/b \to 1$.

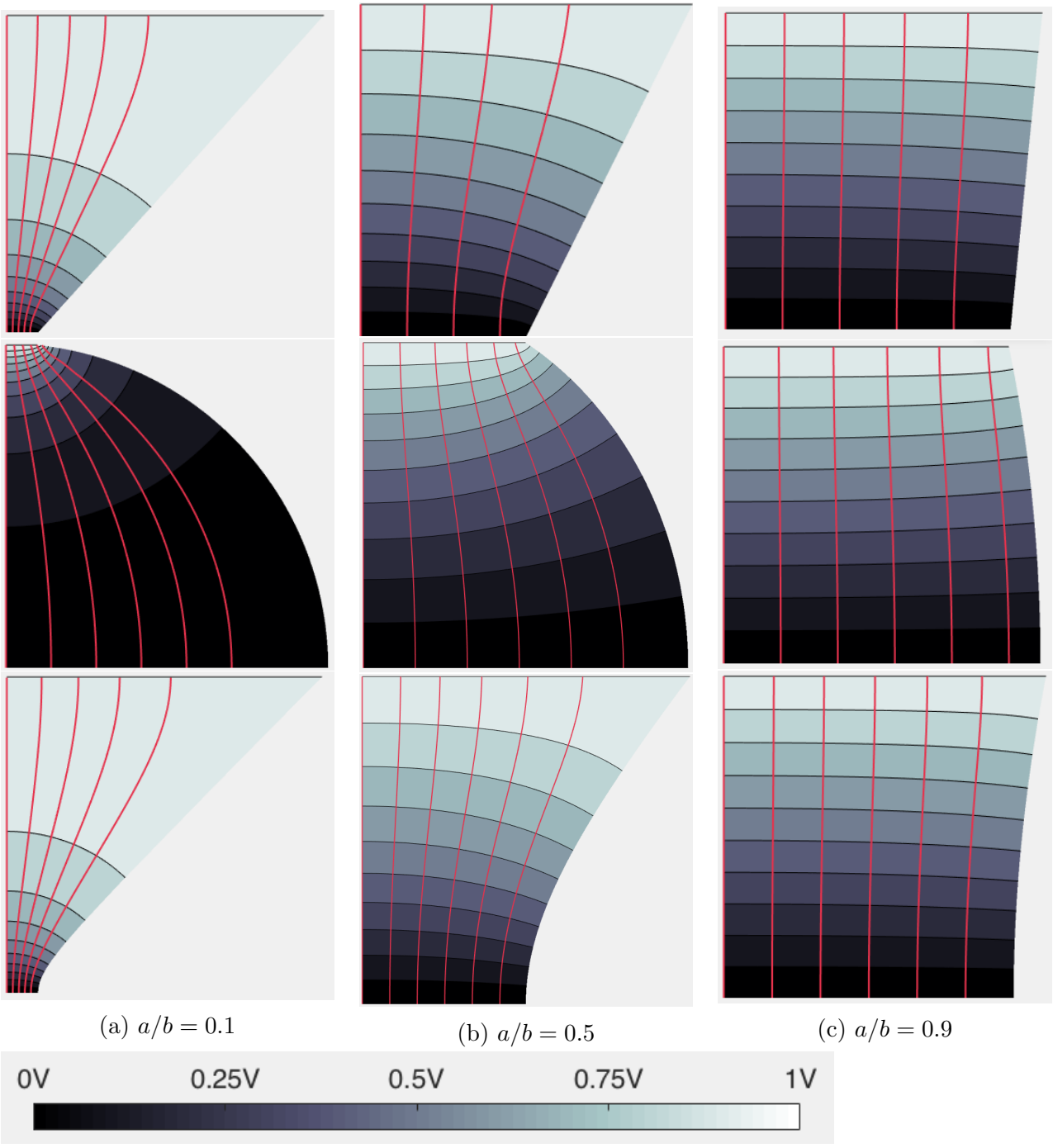

(a) $a/b = 0.1$ (b) $a/b = 0.5$ (c) $a/b = 0.9$

Figure 3.2: Contour plots of the computed electric potential, and the electric field lines (perpendicular to equipotentials), for the truncated conical, ellipsoidal, and hyperboloidal resistors.

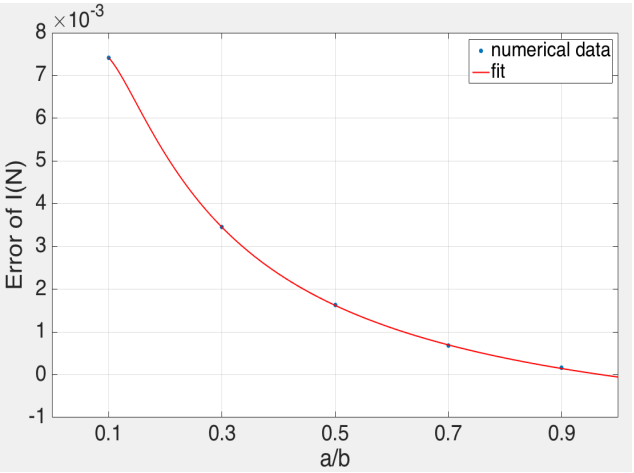

(a) Estimated error of the current in a truncated conical resistor

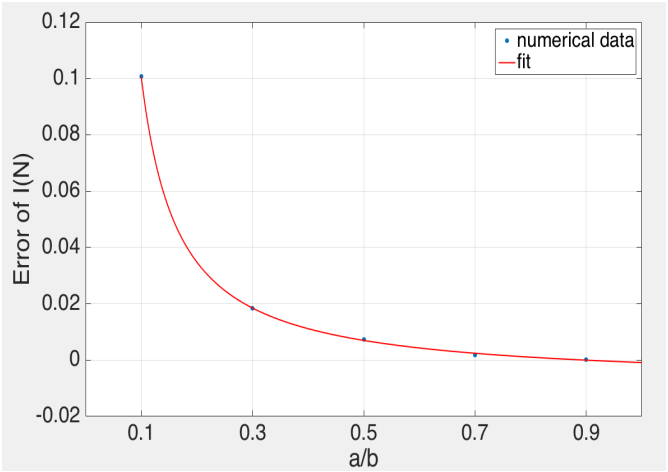

(b) Estimated error of the current in a truncated ellipsoidal resistor

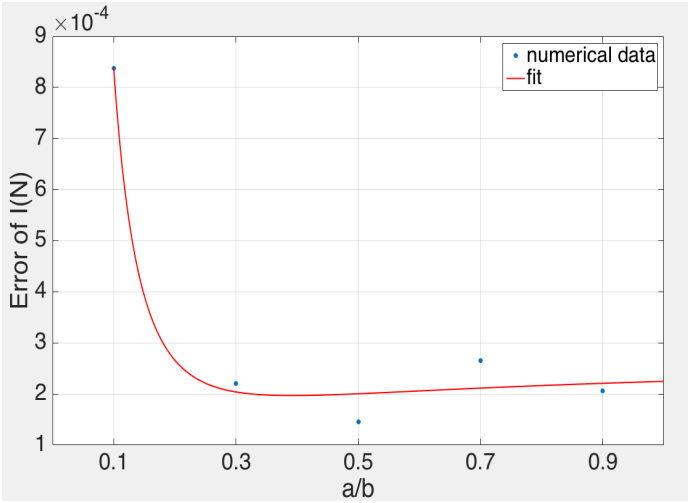

(c) Estimated error of the current in a truncated hyperboloidal resistor

Figure 3.3: The estimated error of the average total current in truncated resistors is larger when $a/b << 1$. The average total current was calculated for $N = 3200$. The red curve is intended as an aid to the eye, to show the trend in the data.

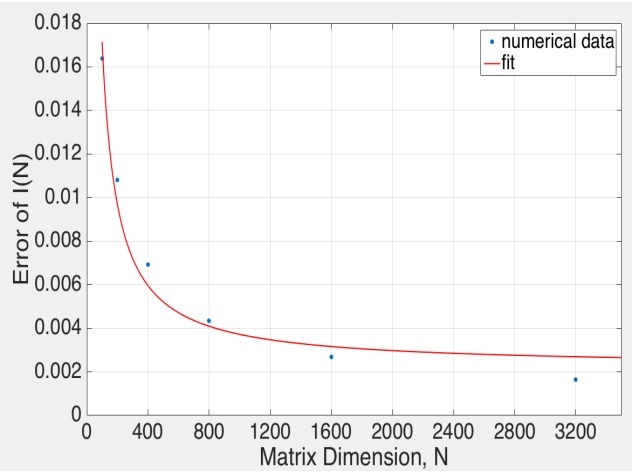

(a) Estimated error of the current in a truncated conical resistor, with $a/b = 0.5$

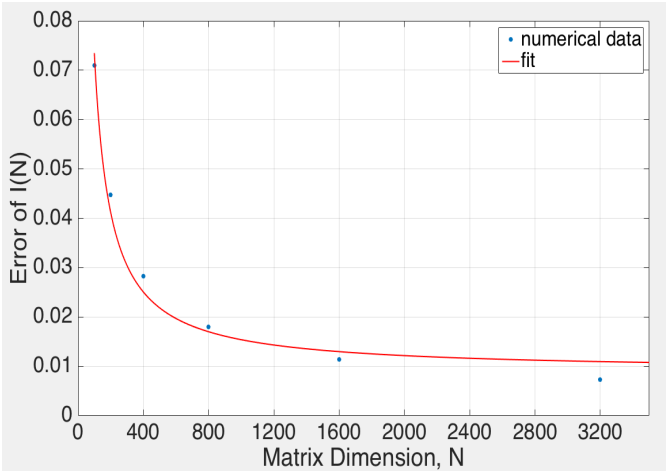

(b) Estimated error of the current in a truncated ellipsoidal resistor, with $a/b = 0.5$

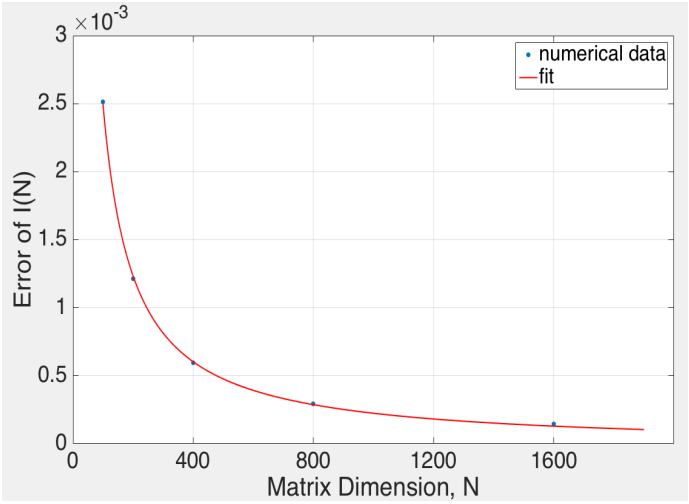

(c) Estimated error of the current in a truncated hyperboloidal resistor, with $a/b = 0.5$

Figure 3.4: Estimated error of the average total current in truncated resistors. The red curve is proportional to $1/N$, it is intended as an aid to the eye, to show the trend in the data.

3.2 Dielectric Breakdown Results

Dielectric breakdown clusters were grown on the honeycomb, square, and triangle lattices, as well as a random distribution of nodes (Fig. 3.6, 3.7, 3.8, and 3.9). The outer circular ring boundary is an electrode surface of constant potential. The central point is where the cluster initial begins to grow. All lattice sites or nodes which belong to the cluster have a potential value of $0V$. The electric potential was calculated according to the methods in section 2.4 and 2.5.

The fractal dimension of the clusters was evaluated using the sandbox method (2.51), the box

counting method (2.52), and the radius of gyration (2.55). The results are listed in Tables 3.1 and 3.2. The fractal dimension was averaged over five clusters for each case, and the error of the calculations was estimated with the standard deviation of the five values.

Figure 3.10 shows how the fractal dimension is extracted from the slope of a least squares fit of the linear portion of data from the sandbox method. The sandbox method works by placing a circle of radius L centered close to the center of mass of the cluster (for symmetric boundary conditions this occurs at the geometric center). While increasing L, the number of sites which belong to the cluster within L, $N(L)$, is recorded. $N(L)$ approaches the total number of sites which belong to the cluster as L approaches the enclosing boundary of the cluster. A program was written to find the optimal portion of data to fit. This was done by fitting different sections of the data to a line and choosing the fit with the smallest value of chi-squared. The center of the circle used in the sand box method is fixed as L increases, but the position of the center can be placed at different sites on the cluster. Each site will have a unique scaling relationship between $N(L)$ and L, so the value of the fractal dimension D will depend on the site in the cluster. Figure 3.11 shows histograms of the fractal dimension sampled at different sandbox centers in the cluster. The histogram gives the frequency a given value of the fractal dimension occurs in the cluster. If the histogram is broad then many values of D_{ML} appear in the cluster and the mass distribution will be non-uniform, because $N(L)$ scales with L differently depending on the location in the cluster. A narrow histogram indicates that the mass distribution is approximately uniform; in such a case the cluster can be treated as a monofractal. The term multifractal refers to clusters which contain many dimensions, and non-uniform mass distributions.

A variation on the sandbox method is to replace L with the radius of gyration, R_G. In this case R_G is calculated during the growth of the cluster, and N is the number of sites which belong to the cluster at any given stage. Figure 3.12 shows examples of how the fractal dimension is extracted from the slope of a line of best fit. Similarly, different sections of the data were fit to a line and the fit with the smallest value of chi-squared was chosen.

Figure 3.13 shows how the fractal dimension is extracted from the slope of a least squares fit of the linear portion of data from the box counting method. Once the cluster finished growing, a grid of cell size $\epsilon = l/L$ was placed over the cluster, completely covering it. The number of cells

which are needed to completely cover the cluster, $N(\epsilon)$, was counted for decreasing cell size, ϵ. The scaling portion of the data occurs for when $a/L \ll \epsilon \ll 1$, where a is the lattice spacing.

Increasing the exponent η decreases the fractal dimension. All three methods to evaluate the fractal dimension agree within their error bounds. The fractal dimension is not affected by the number of nearest neighbours; the dimension of the cluster is independent of lattice type it was grown on. This is illustrated by the similar branching structure across lattice types for a constant value of η. The symmetry of the clusters is a reflection of their circular boundary conditions. In Fig. 3.14 and 3.15 the symmetric boundary conditions have been altered to produce clusters which display more directed growth towards high electric potential. This forces the growth process to spend less time creating branches in directions of lower potential, and reduces the fractal dimension of the cluster. Symmetric boundary conditions cause an initial ambiguity in branching direction, which is globally preserved throughout the growth. Locally some branching will grow in preferred directions depending on the local electric field configuration.

The random distribution of nodes was created by perturbing the (x, y) coordinates of the square lattice by a number randomly selected from the interval $[-0.5a, 0.5a]$ or $[-a, a]$, where a is the lattice spacing of the square lattice. The number density of nodes is constant, but selecting from a larger interval generates a distribution with large gaps between nodes. If Δa is relatively small, then on average there will be less nodes within the neighbourhood shell due to the large gaps between nodes (Fig. 2.3). In this case many nodes will have 0 nearest neighbours. As the value of Δa increases, more nodes on average are included within the neighbourhood, and every node will have at least 1 nearest neighbour. If a node in the distribution has 0 nearest neighbours then the potential does not change at that node, and it is treated as a potential boundary. Figure 3.5 (d) and (e) show potential solutions when 2% and 4% of the total nodes have 0 nearest neighbours. The cluster will not grow into nodes with 0 nearest neighbours. These nodes are isolated from the rest of the distribution, and are never included in the perimeter (possible growth nodes) of the cluster. Increasing the percentage of nodes with 0 nearest neighbours creates potential barriers in the distribution that the cluster must grow around (similar to water flowing around boulders), causing more directed growth with less branching and a lower fractal dimension. Table 3.2 shows how the fractal dimension of the clusters decreases when the percentage of nodes with 0 nearest

neighbours increases.

Figure 3.6 shows examples of dielectric breakdown clusters grown on a random distribution of nodes. Increasing Δa reduces the accuracy of the potential calculation using equation (2.28), as discussed in detail at the end of section 2.5. The fractal dimension is unaffected by increasing Δa up to $0.75a$, as compared with the results for when $\Delta a = 0$. The plot of the potential solution in Fig. 3.5 also confirms that increasing Δa up to $0.75a$ does not significantly change the results. The electric potential must be solved accurately enough so that a free branch tip is assigned a higher growth probability (2.50) than the branch tips which are trying to grow in regions between branches. The electric field is stronger in the neighbourhood of free branch tips, as they are further from the cluster (0V) and closer to the boundary (1V). The branches screened by the cluster feel a weaker electric field and are not as likely to grow. The heat-map of the potential in Fig. 3.5 shows that the computed solution is able to resolve the "tip effect" and "Faraday screening"[12]. Free branch tips, far from the center of mass of the cluster, display a larger gradient in the potential than screened regions.

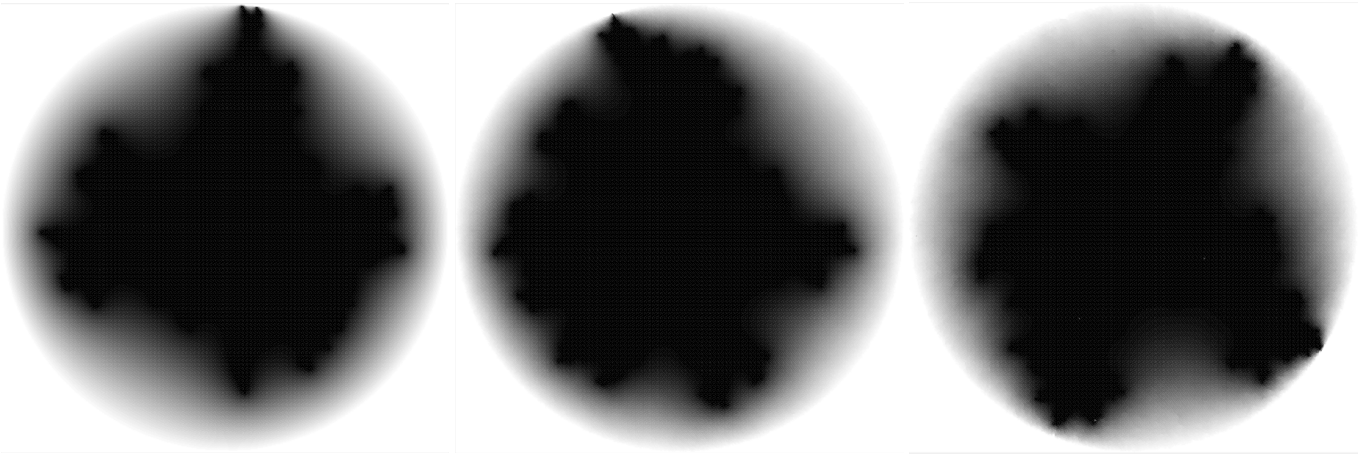

(a) $\Delta a = 0$, 0% of nodes with 0 n.n's.

(b) $\Delta a = 0.75a$, 0% of nodes with 0 n.n's.

(c) $\Delta a = 0.5a$, 0.003% of nodes with 0 n.n's.

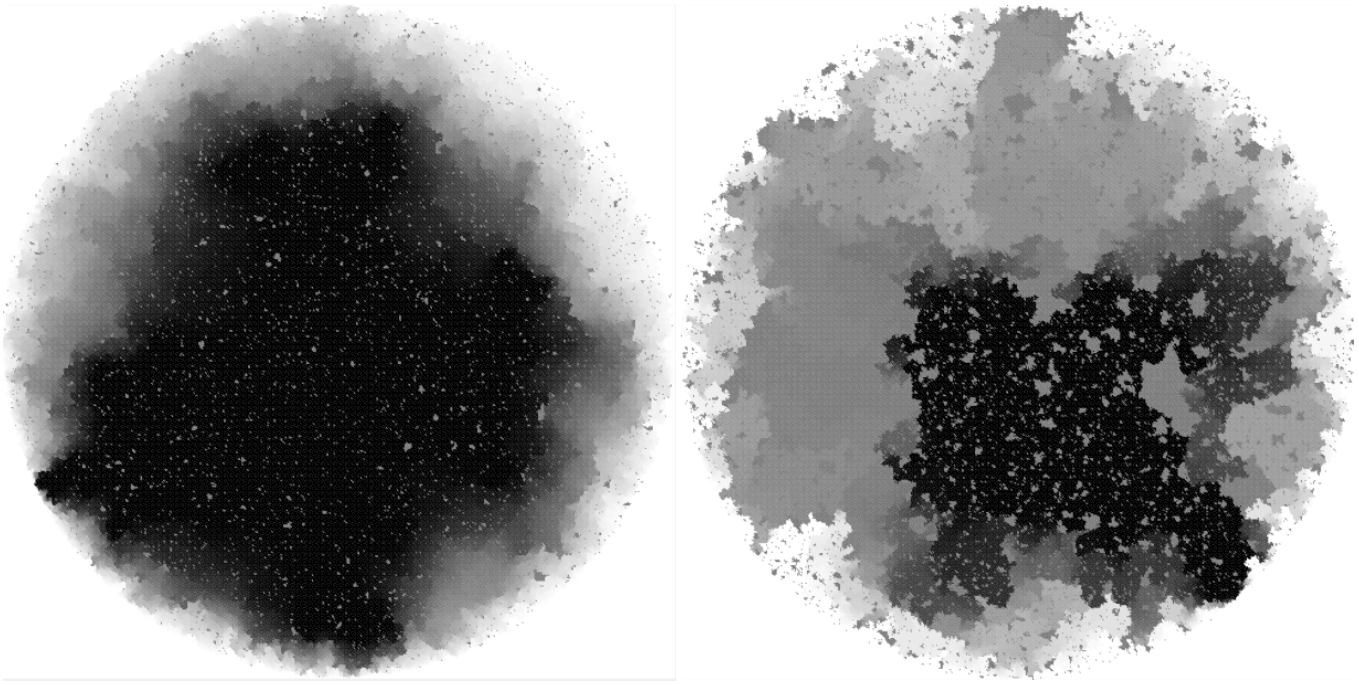

(d) $\Delta a = 0.25a$, 2% of nodes with 0 n.n's.

(e) $\Delta a = 0.25a$, 4% of nodes with 0 n.n's.

Figure 3.5: A visualization of the potential solutions to Laplace's equation on a random distribution of nodes is figured here. The black regions are 0V and white are 1V.

The singularity spectra were calculated for the square lattice and random distribution of nodes (Fig. 3.16 and 3.17) according to the methods in section 2.9.1. The maximum of the $f(\alpha)$ curve is the fractal dimension as calculated by the box counting method, and occurs when $q = 0$. The range of α values, $\Delta\alpha = \alpha_{max} - \alpha_{min}$, provides a measure of the multifractality of the cluster. when $\Delta\alpha$ is large the mass distribution is non-uniform with many singularities of different strengths (values of α). When $\Delta\alpha$ is small the mass distribution is uniform, and is represented with a

single singularity strength, α. For the dielectric breakdown clusters grown on the square lattice, $\Delta\alpha \sim 0.086$, which suggests the clusters are monofractals, with a uniform mass distribution. For the dielectric breakdown clusters grown on a random distribution of nodes, $\Delta\alpha$ is small, which again suggests that the clusters are monofractals with a uniform mass distribution.

The generalized dimension spectra were calculated for the square lattice and random distribution of nodes (Fig. 3.18) according to the methods in section 2.9.1. The value of D_q at $q = 0$ is the fractal dimension as calculated by the box counting method, and $D_{-\infty}$ is the fractal dimension as calculated by the sandbox method [13]. This is seen by considering that in Fig. 3.18 the value of D_{-5} is approximately equal to D_{ML} found in Table 3.1. The sandbox method always produces a fractal dimension larger than the box counting method. The difference between the two methods $[D_{-\infty} - D_0]$ measures the non-uniformity of the mass distribution in the cluster. The value of q changes the sum, $\chi_q(\epsilon)$, in (2.58). Large positive values of q magnify dense regions of the cluster ($p_i \sim 1$), and large negative values of q magnify rarer regions of the cluster ($p_i \ll 1$). If the value of $\chi_q(\epsilon)$ is independent of changes in q then all D_q's will be the same. This means that the mass is distributed uniformly in the cluster (i.e. $D_{-5} \approx D_0$ or $D_{ML} \approx D_{BOX}$). The generalized dimension spectra in Fig. 3.18 are approximately horizontal. This is reflected in the agreement between sandbox and box counting methods to calculate the fractal dimension. Thus the cluster's mass distributions are uniform, and they are monofractals.

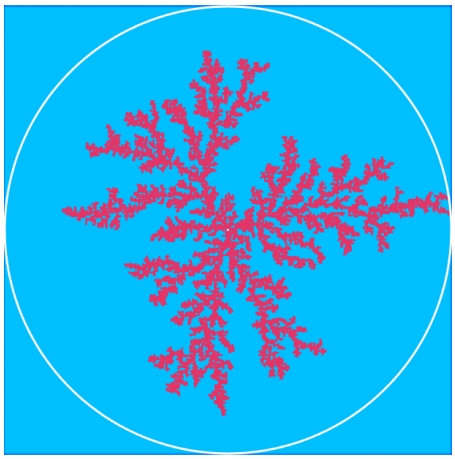

(a) $D \sim 1.68$, $\Delta a = 0$, <n.n>= 4, 0% of nodes with 0 n.n's

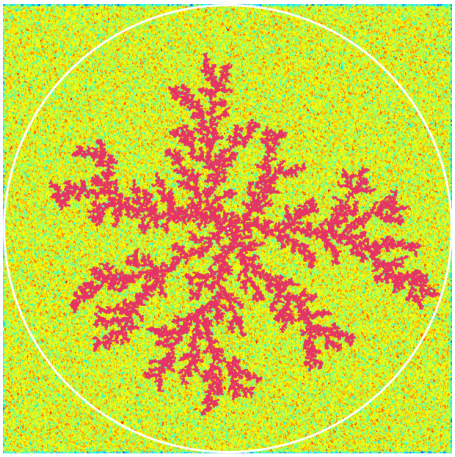

(b) $D \sim 1.687$, $\Delta a = 0.75a$, <n.n>= 8.55, 0% of nodes with 0 n.n's

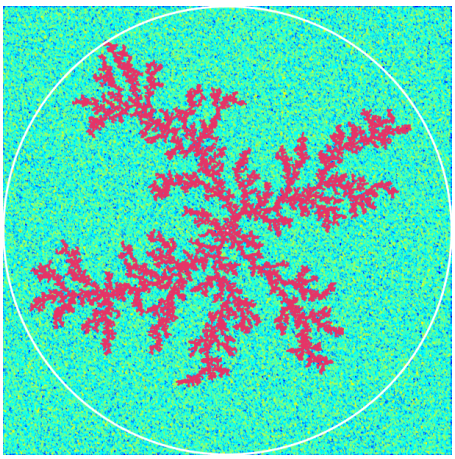

(c) $D \sim 1.669$, $\Delta a = 0.5a$, <n.n>= 5.74, 0.003% of nodes with 0 n.n's

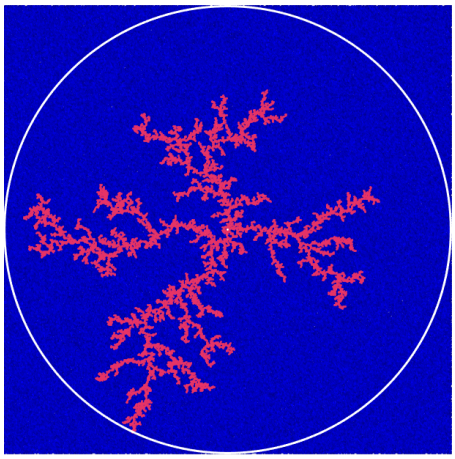

(d) $D \sim 1.55$, $\Delta a = 0.25a$, <n.n>= 2.94, 2% of nodes with 0 n.n's

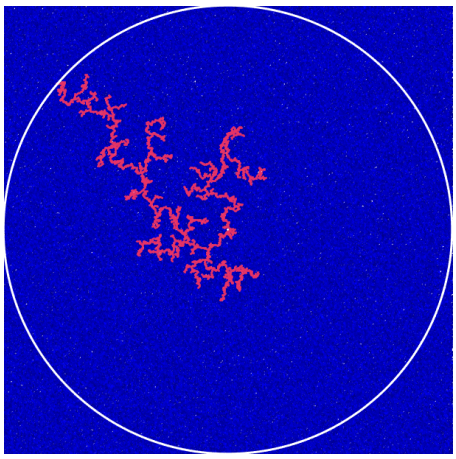

(e) $D \sim 1.38$, $\Delta a = 0.25a$, <n.n>= 2.79, 4% of nodes with 0 n.n's

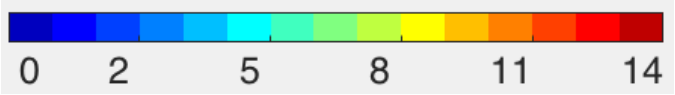

Figure 3.6: This figure shows dielectric breakdown cluster generated on a random distribution of nodes. The nodes are created by perturbing each (x, y) coordinate of the square lattice by a number randomly selected from the interval $[-0.5a, 0.5a]$, or $[-a, a]$, where a is the lattice spacing of the square lattice, and Δa is the size of the neighbourhood shell (see Fig. 2.3). The variation in the background colour of the image represents the variation in the number of nearest neighbours for each node in the distribution. In the image (a) every node has 4 nearest neighbours, so the background is a solid blue colour. In images (b) - (e) there is variation in the number of nearest neighbours for different nodes, so the background appears pixelated with a mixture of blue and yellow pixels. The colour associated with number of nearest neighbours is shown in the colour bar. As the percentage of nodes which have 0 nearest neighbours increases, the fractal dimension decreases. The fractal dimension was determined by the box counting method.

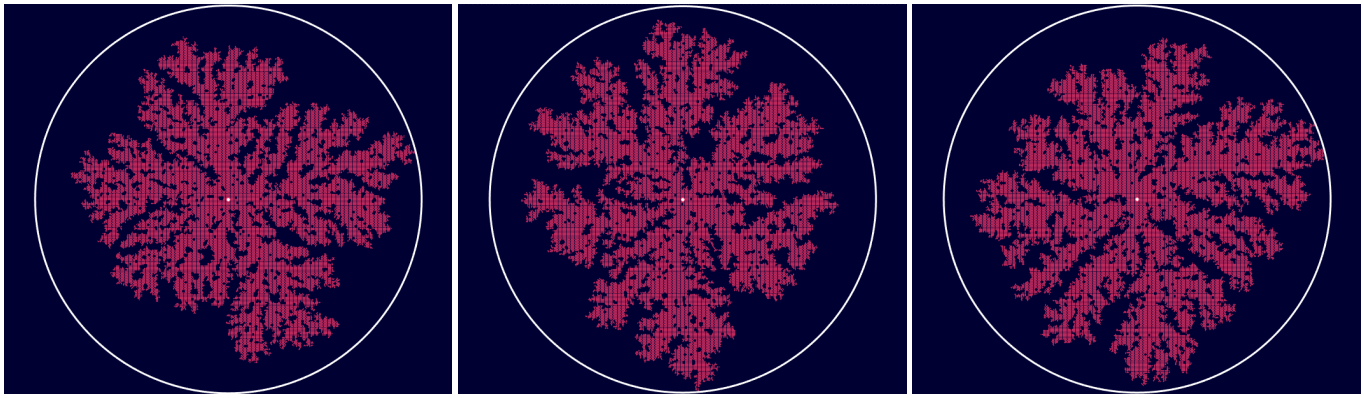

(a) $\eta = 0.5$, $D \approx 1.889$

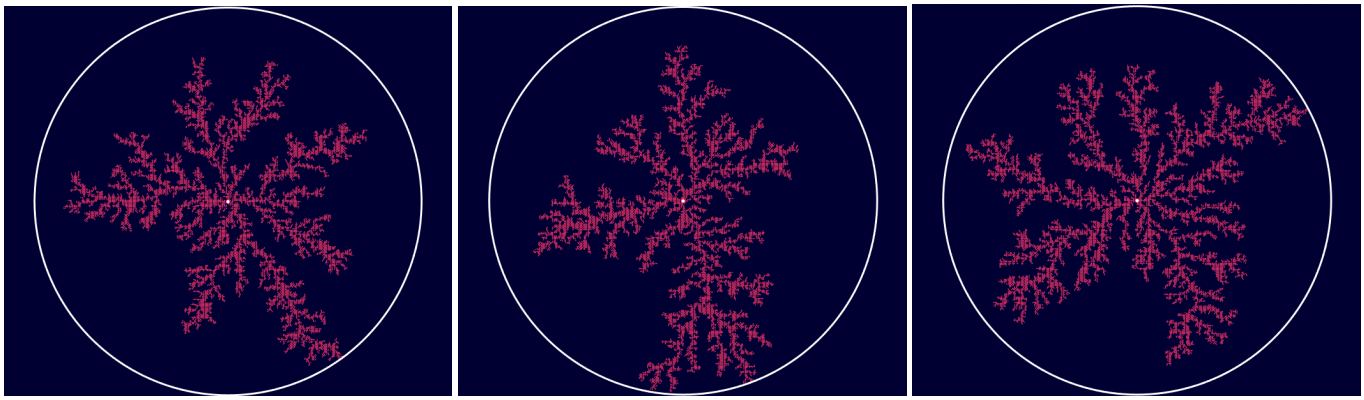

(b) $\eta = 1$,$D \approx 1.673$

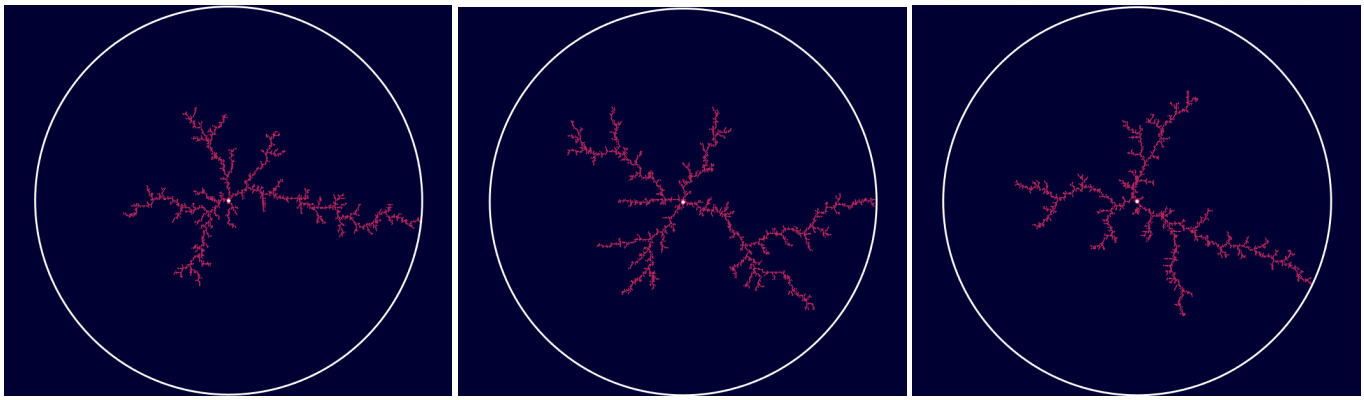

(c) $\eta = 2$, $D \approx 1.39$

Figure 3.7: Three separate examples of dielectric breakdown clusters grown on a honeycomb lattice (3 nearest neighbours). The fractal dimension, D, decreases with increasing the exponent, η; in the relation between probability and the local electric field (2.50). The outer ring was kept at $1V$, and every lattice that belongs to the cluster has a potential of $0V$. The fractal dimension was determined by the box counting method.

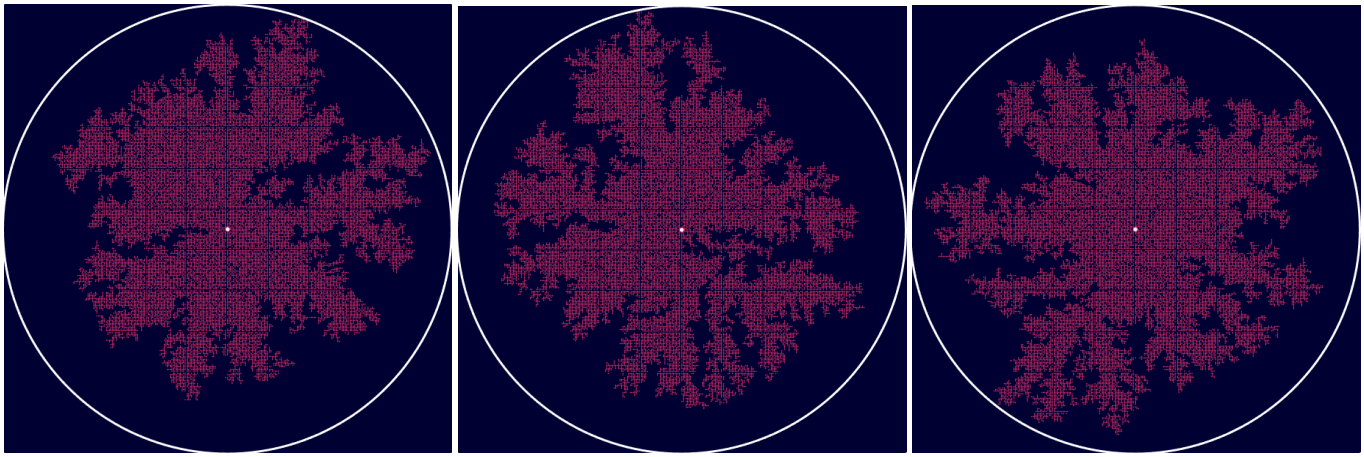

(a) $\eta = 0.5$, $D \approx 1.908$

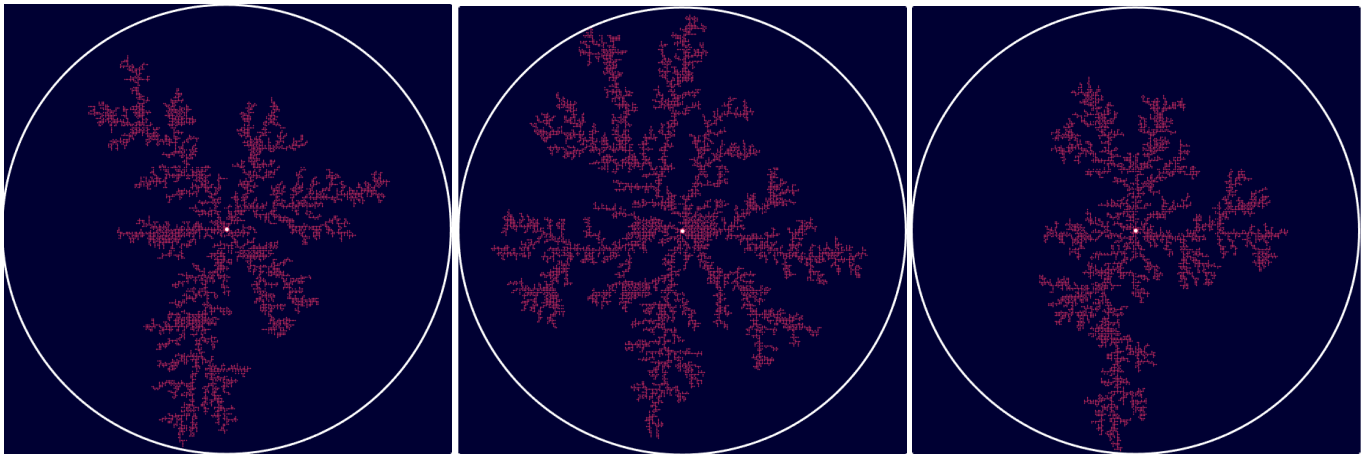

(b) $\eta = 1$,$D \approx 1.68$

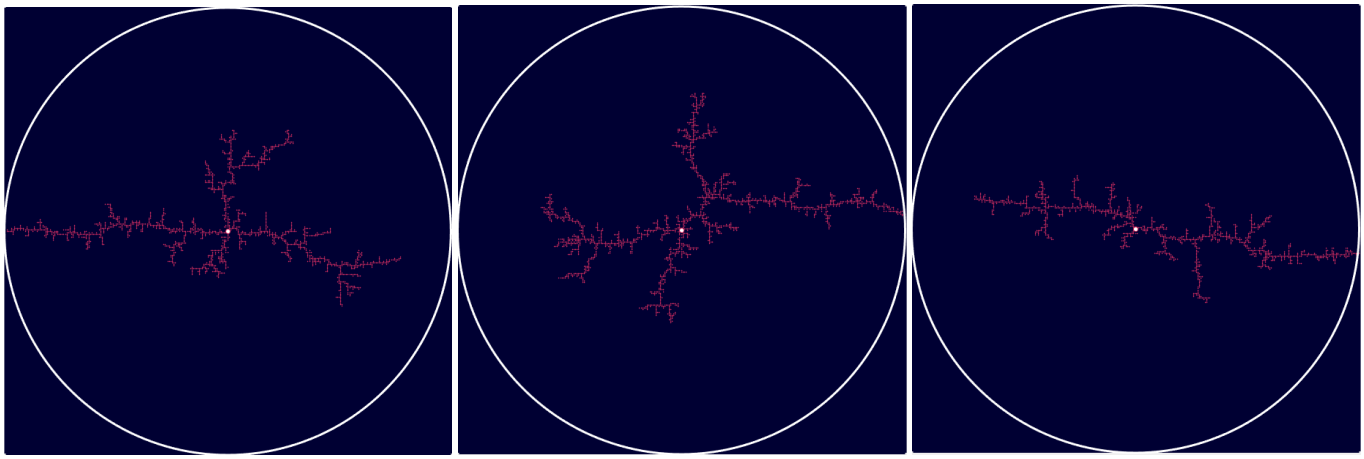

(c) $\eta = 2$, $D \approx 1.386$

Figure 3.8: Three separate examples of dielectric breakdown clusters grown on a square lattice (4 nearest neighbours). The fractal dimension, D, decreases with increasing the exponent, η; in the relation between probability and the local electric field (2.50). The outer ring was kept at $1V$, and every lattice that belongs to the cluster has a potential of $0V$. The fractal dimension was determined by the box counting method.

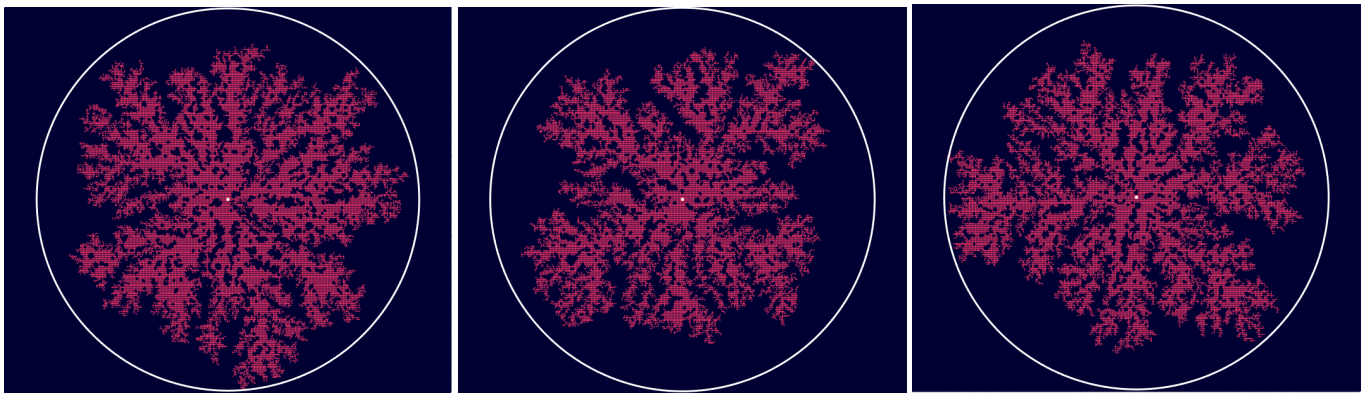

(a) $\eta = 0.5$, $D \approx 1.88$

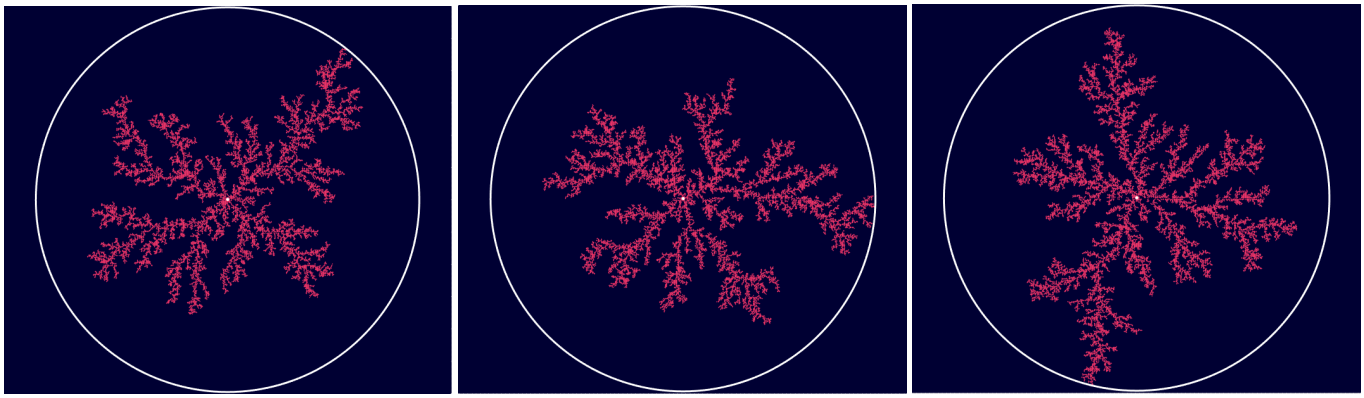

(b) $\eta = 1$,$D \approx 1.667$

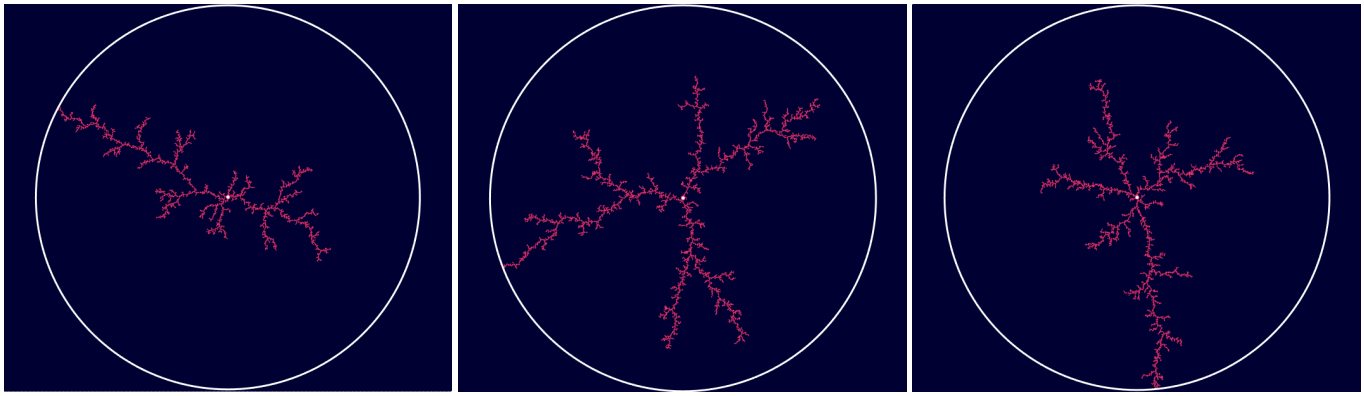

(c) $\eta = 2$, $D \approx 1.372$

Figure 3.9: Three separate examples of dielectric breakdown clusters grown on a triangular lattice (6 nearest neighbours). The fractal dimension, D, decreases with increasing the exponent, η; in the relation between probability and the local electric field (2.50). The outer ring was kept at $1V$, and every lattice that belongs to the cluster has a potential of $0V$. The fractal dimension was determined by the box counting method.

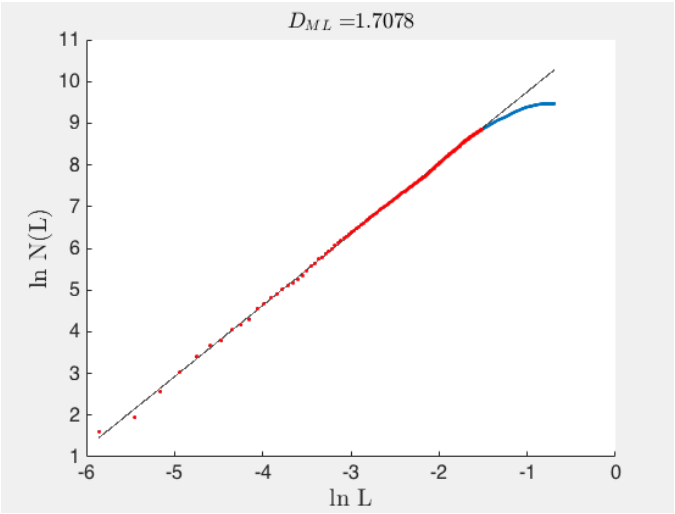

(a) Triangular lattice, $\eta = 1$.

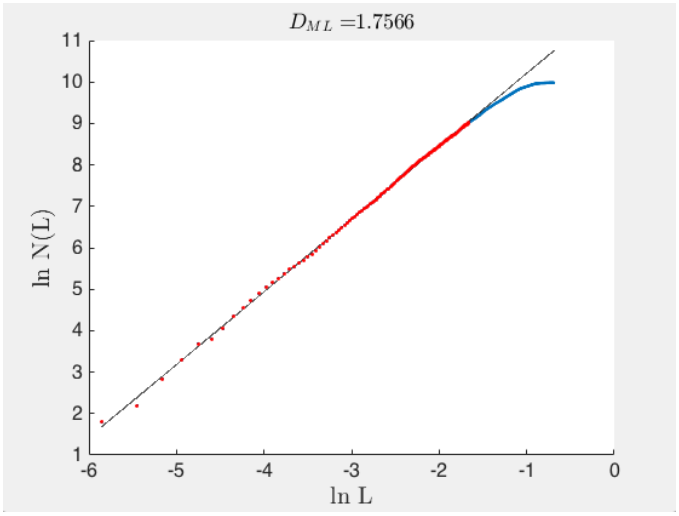

(b) Square lattice, $\eta = 1$

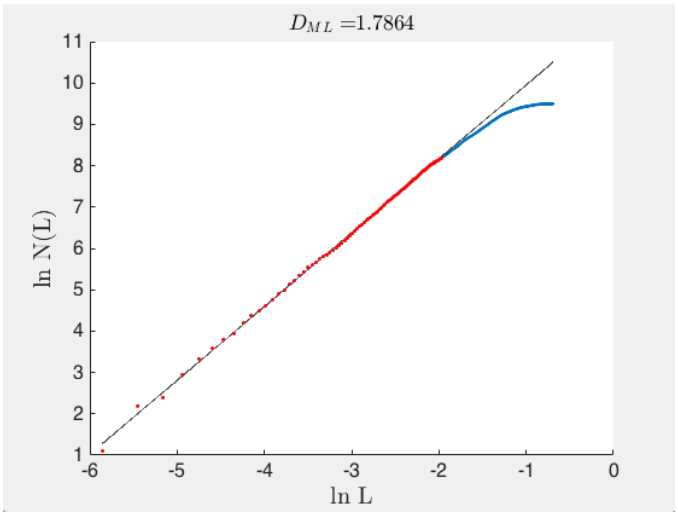

(c) Honeycomb lattice, $\eta = 1$

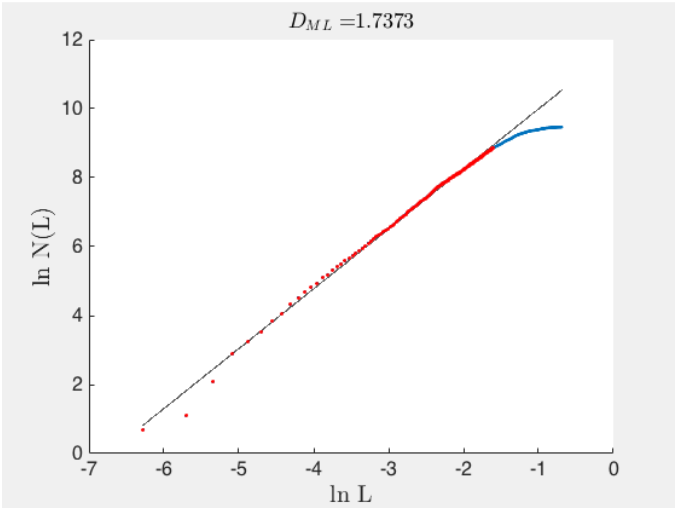

(d) Random distribution of nodes, $\eta = 1$, 0.003% of nodes with 0 n.n's

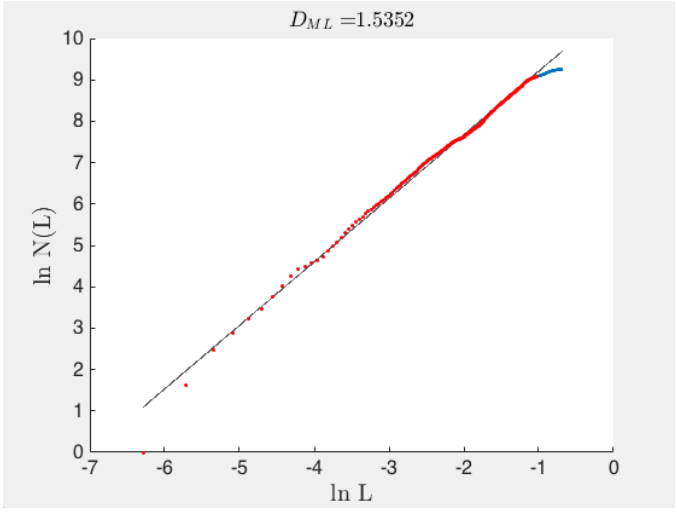

(e) Random distribution of nodes, $\eta = 1$, 2% of nodes with 0 n.n's

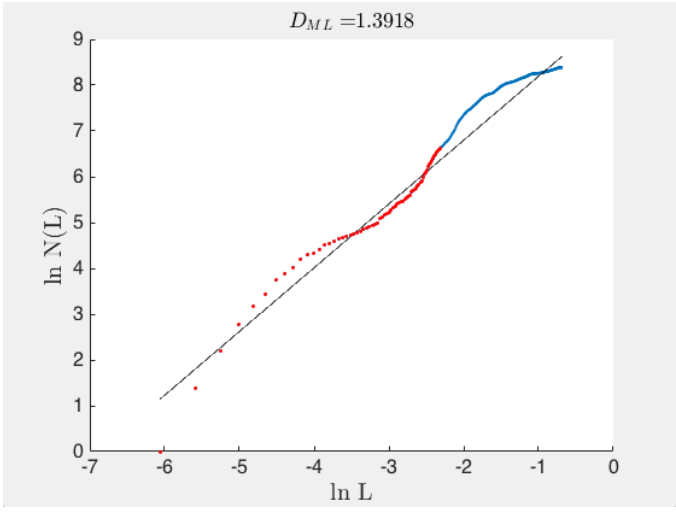

(f) Random distribution of nodes, $\eta = 1$, 4% of nodes with 0 n.n's

Figure 3.10: This figure shows the method of determining the fractal dimension from the slope of a log-log plot of $(\ln(L), \ln N(L))$ (see section 2.9). The data in these plots were averaged over five clusters for each lattice type.

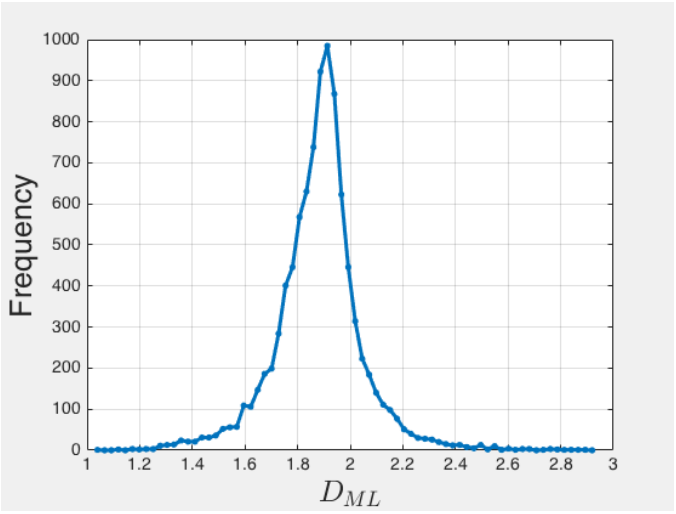

(a) Square lattice, $\eta = 0.5$, 22983 breaks, 10000 samples.

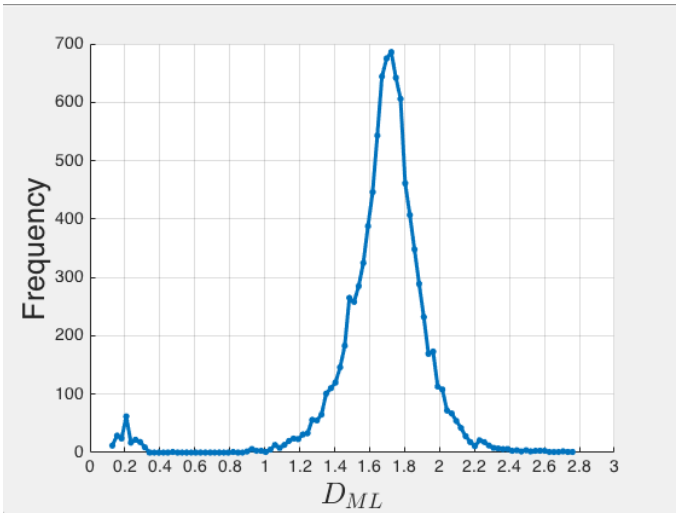

(b) Square lattice, $\eta = 1$, 18470 breaks, 10000 samples.

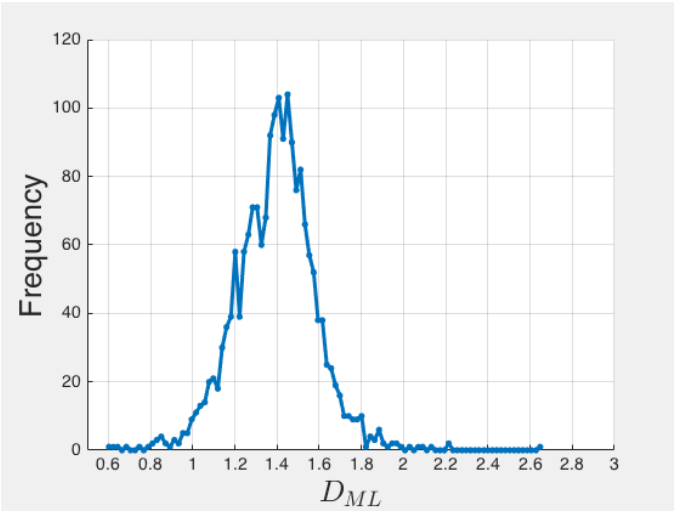

(c) Square lattice, $\eta = 2$, 4471 breaks, 2000 samples.

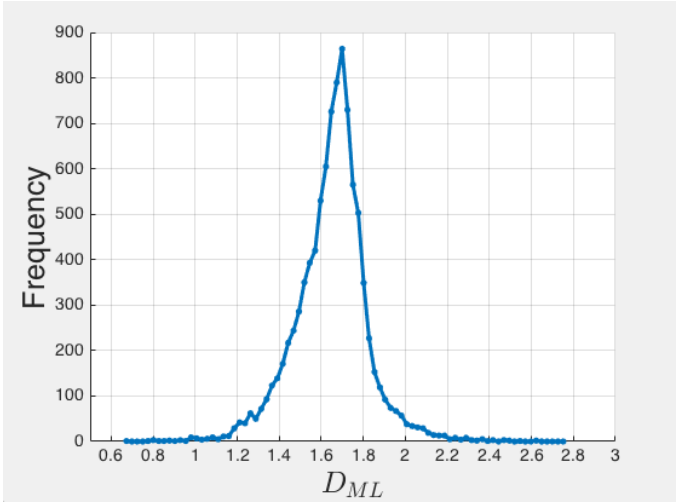

(d) Random distribution of nodes, $\eta = 1$, 0.003% of nodes with 0 n.n's, 15796 breaks, 10000 samples.

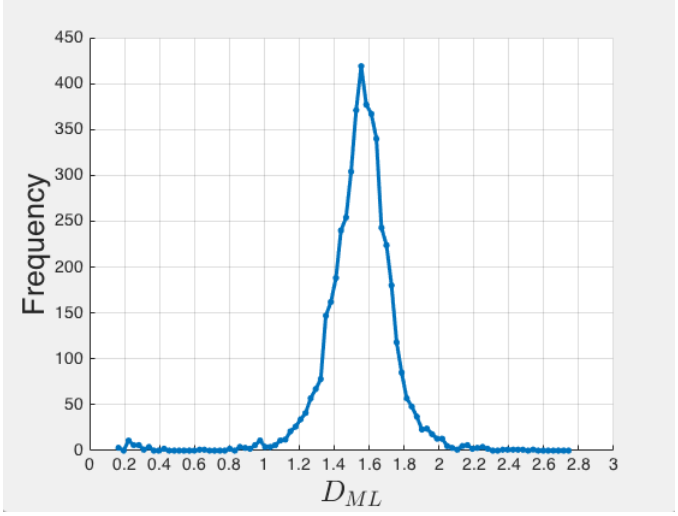

(e) Random distribution of nodes, $\eta = 1$, 2% of nodes with 0 n.n's, 10431 breaks, 5000 samples.

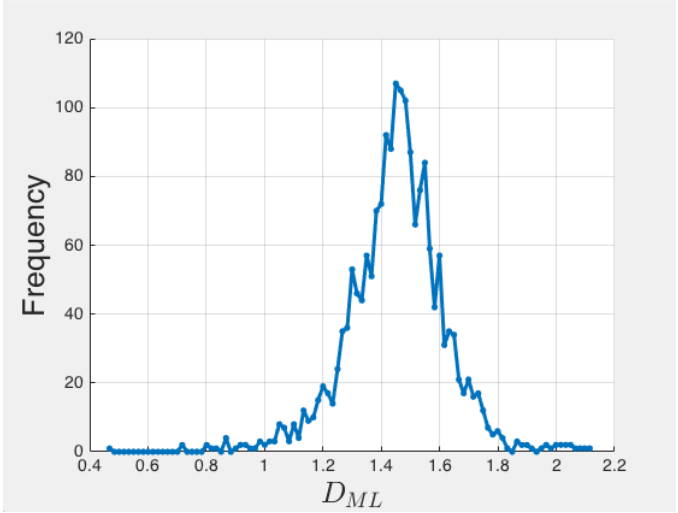

(f) Random distribution of nodes, $\eta = 1$, 4% of nodes with 0 n.n's, 4385 breaks, 2000 samples.

Figure 3.11: This figure shows the frequency with which certain values of the fractal dimension occur. A number of sites on the cluster were sampled with the sand box method. The most frequent value of D_{ML} in the cluster is the value the sand box method gives when the center of the circle is at the center of mass.

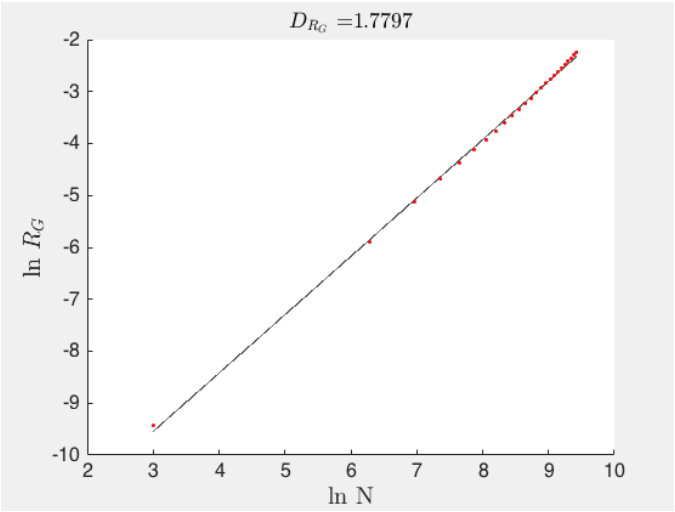

(a) Triangular lattice, $\eta = 1$.

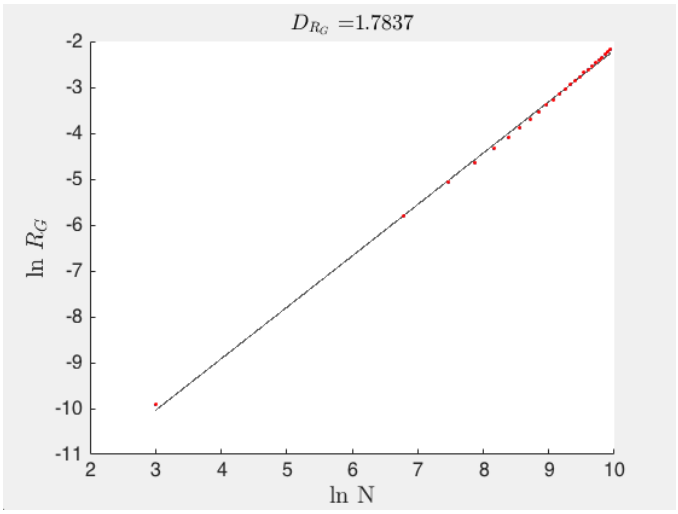

(b) Square lattice, $\eta = 1$

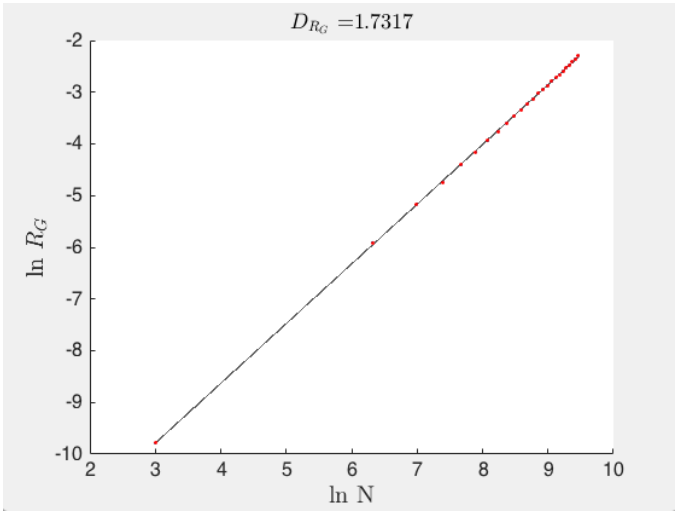

(c) Honeycomb lattice, $\eta = 1$

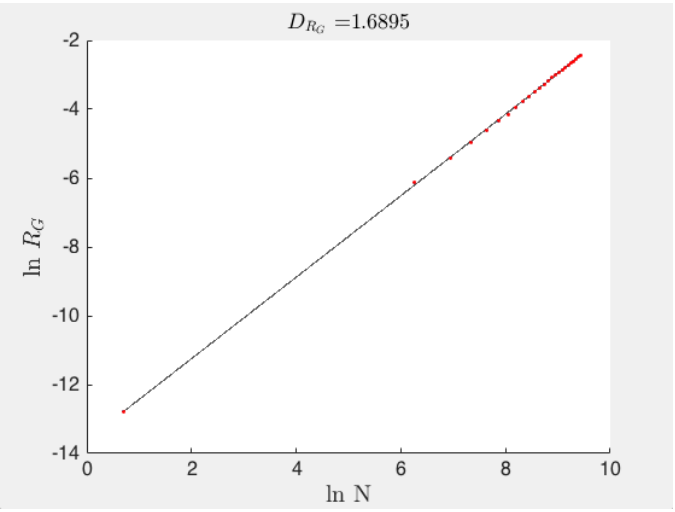

(d) Random distribution of nodes, $\eta = 1$, 0.003% of nodes with 0 n.n's

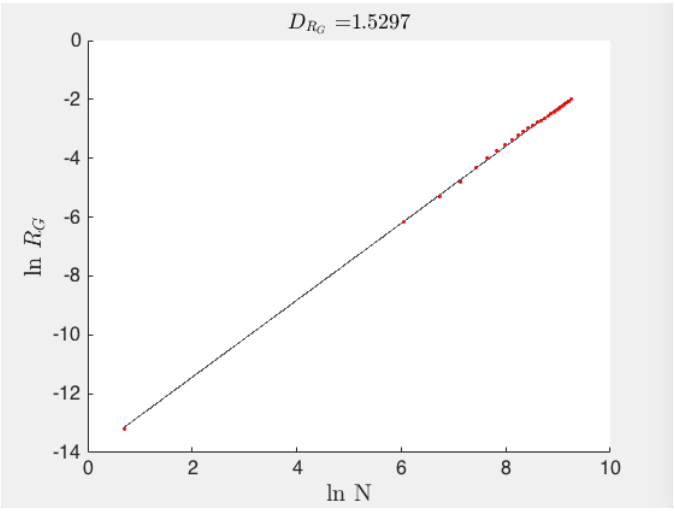

(e) Random distribution of nodes, $\eta = 1$, 2% of nodes with 0 n.n's

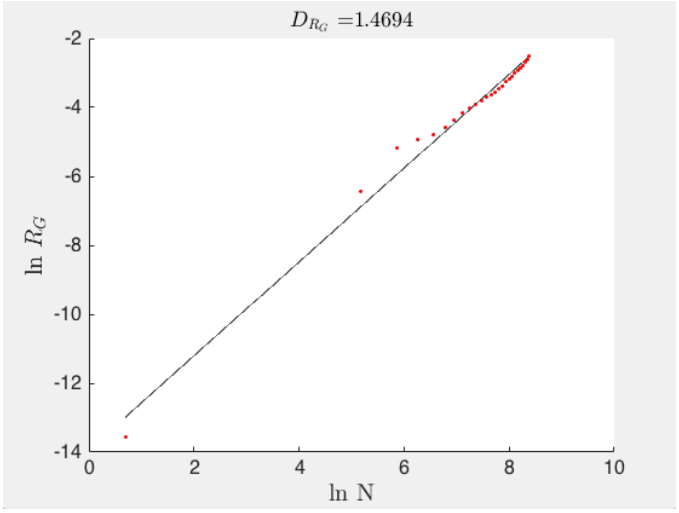

(f) Random distribution of nodes, $\eta = 1$, 4% of nodes with 0 n.n's

Figure 3.12: This figure shows the method of determining the fractal dimension from the slope of a log-log plot of $(\ln N, \ln R_G)$ (see section 2.9). The data in these plots were averaged over five clusters for each lattice type.

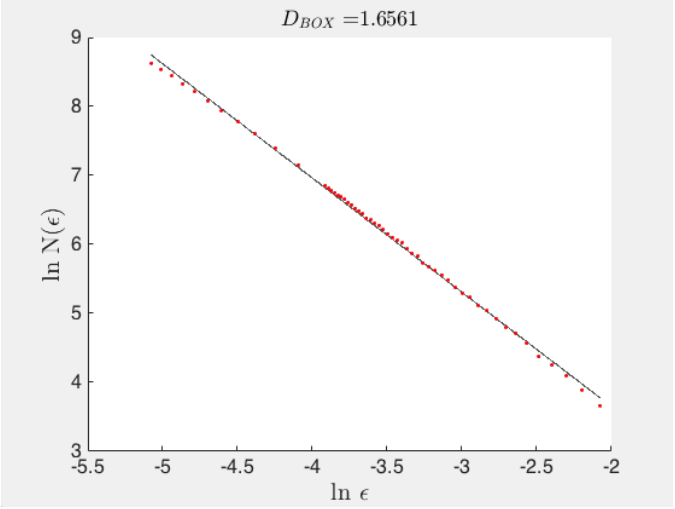

(a) Triangular lattice, $\eta = 1$.

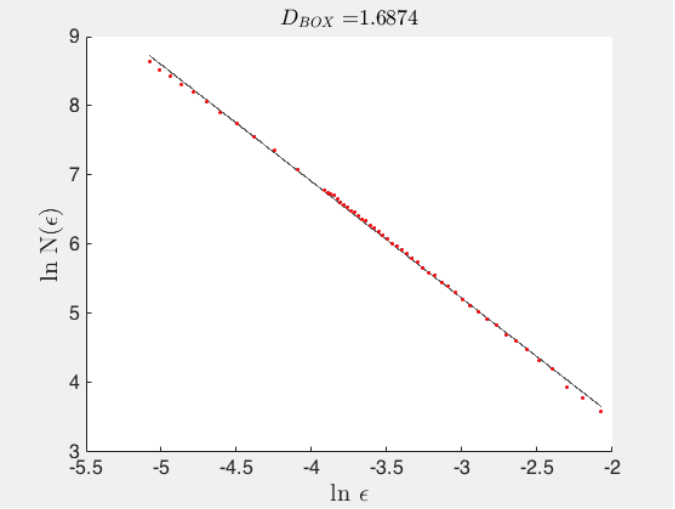

(b) Square lattice, $\eta = 1$

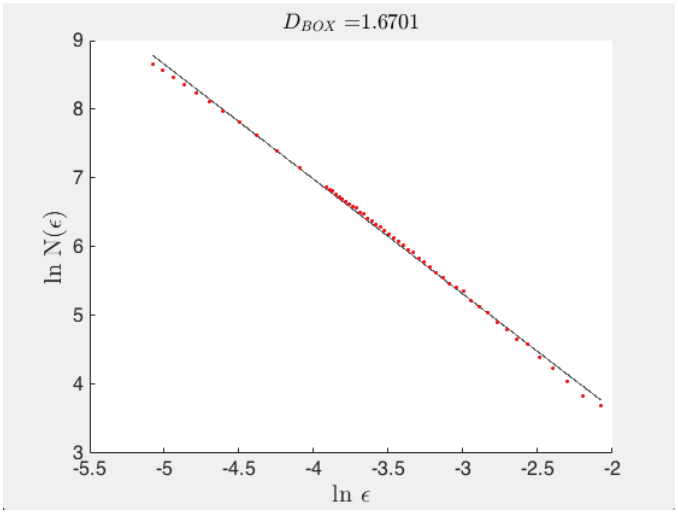

(c) Honeycomb lattice, $\eta = 1$

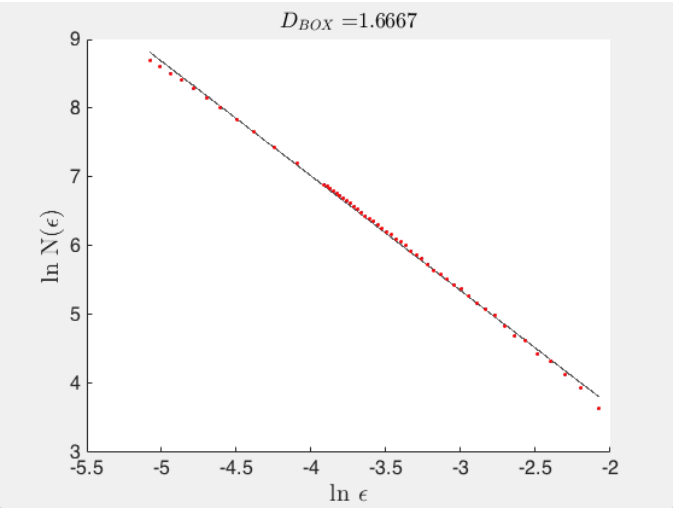

(d) Random distribution of nodes, $\eta = 1$, 0.003% of nodes with 0 n.n's

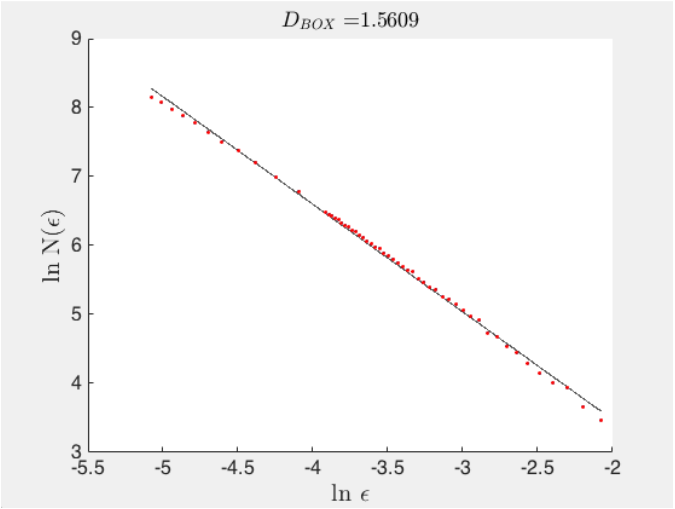

(e) Random distribution of nodes, $\eta = 1$, 2% of nodes with 0 n.n's

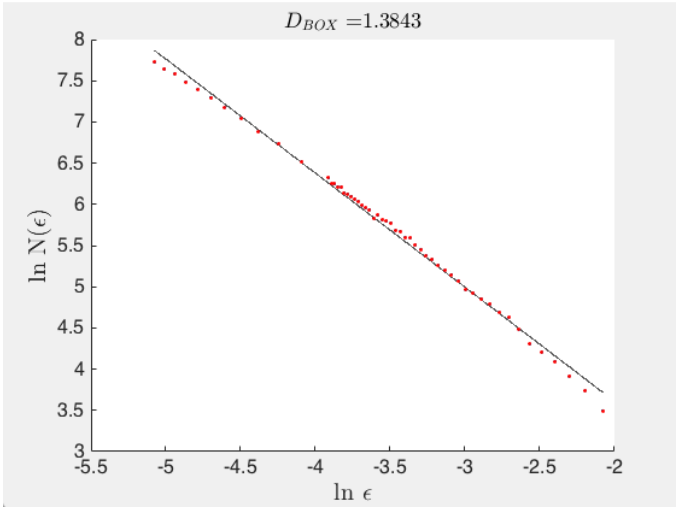

(f) Random distribution of nodes, $\eta = 1$, 4% of nodes with 0 n.n's

Figure 3.13: This figure shows the method of determining the fractal dimension from the slope of a log-log plot of $(\ln \epsilon, \ln N(\epsilon))$ (see section 2.9). The data in these plots were averaged over five clusters for each lattice type.

η	no. n.n's	D_{ML}	D_{R_G}	D_{BOX}
0.5	3	1.894 ± 0.008	1.91 ± 0.01	1.889 ± 0.005
	4	1.900 ± 0.009	1.94 ± 0.04	1.908 ± 0.003
	6	1.88 ± 0.03	1.93 ± 0.03	1.88 ± 0.01
1	3	1.73 ± 0.03	1.75 ± 0.04	1.673 ± 0.007
	4	1.71 ± 0.03	1.74 ± 0.04	1.68 ± 0.01
	6	1.71 ± 0.02	1.76 ± 0.05	1.667 ± 0.008
2	3	1.46 ± 0.07	1.40 ± 0.07	1.39 ± 0.01
	4	1.43 ± 0.06	1.45 ± 0.04	1.386 ± 0.009
	6	1.53 ± 0.03	1.45 ± 0.07	1.372 ± 0.006

Table 3.1: Fractal dimension of DBM clusters grown on the honeycomb (3 n.n's), square (4 n.n's), and triangular (6 n.n's) lattice. D_{R_G} is the fractal dimension as calculated by the radius of gyration method. D_{ML} is calculated with the sandbox method using the mass-length relation. D_{BOX} is calculated by the box counting method. The statistical error is estimated by averaging results over five clusters for each lattice.

Interval	Δa	<n.n>	% of nodes with 0 n.n's	D_{ML}	D_{R_G}	D_{BOX}
$[0, 0]$	0	4	0	1.71 ± 0.03	1.74 ± 0.04	1.68 ± 0.01
$[-0.5a, 0.5a]$	$0.75a$	8.55	0	1.71 ± 0.03	1.77 ± 0.06	1.687 ± 0.007
$[-0.5a, 0.5a]$	$0.5a$	5.74	0.003	1.71 ± 0.02	1.68 ± 0.04	1.669 ± 0.006
$[-0.5a, 0.5a]$	$0.25a$	2.94	2	1.54 ± 0.06	1.6 ± 0.1	1.55 ± 0.01
$[-a, a]$	$0.25a$	2.79	4	1.50 ± 0.09	1.6 ± 0.1	1.38 ± 0.01

Table 3.2: Fractal dimension of DBM clusters grown on a random distribution of nodes. D_{R_G} is the fractal dimension as calculated by the radius of gyration method. D_{ML} is calculated with the sandbox method using the mass-length relation. D_{BOX} is calculated by the box counting method. The statistical error is estimated by averaging results over five clusters. The nodes are created by perturbing each (x, y) coordinate of the square lattice by a number randomly selected from the interval $[-0.5a, 0.5a]$ or $[-a, a]$, where a is the lattice spacing of the square lattice. The number density of nodes is constant, but selecting from a larger interval generates larger gaps between nodes. If Δa is relatively small, then on average there will be less nodes within the neighbourhood due to the large gaps between nodes. In this case many nodes will have 0 nearest neighbours. As the value of Δa increases, more nodes on average are included within the neighbourhood, and every node has at least 1 nearest neighbour. When the % of nodes with 0 nearest neighbours increases the fractal dimension decreases.

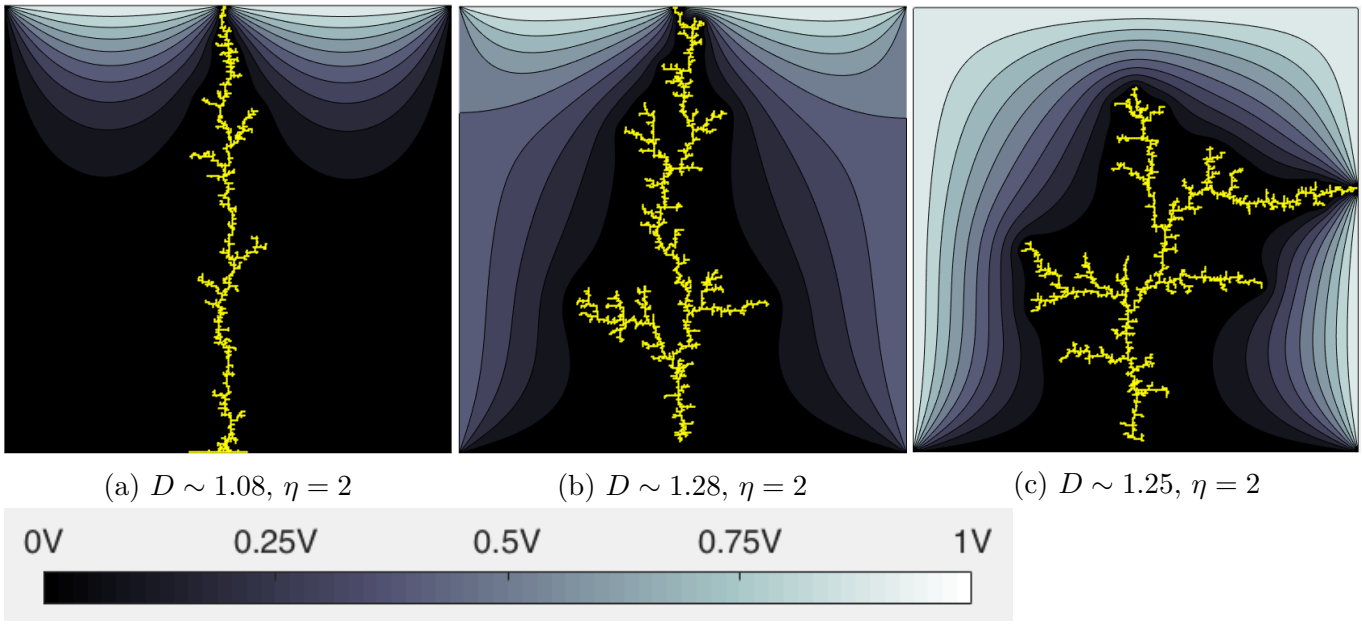

(a) $D \sim 1.08$, $\eta = 2$ (b) $D \sim 1.28$, $\eta = 2$ (c) $D \sim 1.25$, $\eta = 2$

Figure 3.14: These clusters were grown on the square lattice. In (a) three boundaries of the square are set to a potential of $V = 0$. The cluster shows highly directional growth to the top of the lattice, where $V = 1$, and a has a fractal dimension, D, close to one. In (b) two opposing boundaries are set to $V = 0.5$, and in (c) $V = 1$. As the potential on opposing boundaries is increased, the cluster growth is more dispersive, with increased branching, and D relatively increases.The clusters are superimposed on a contour plot of the electric potential, defined by $E = -\nabla\Phi$.

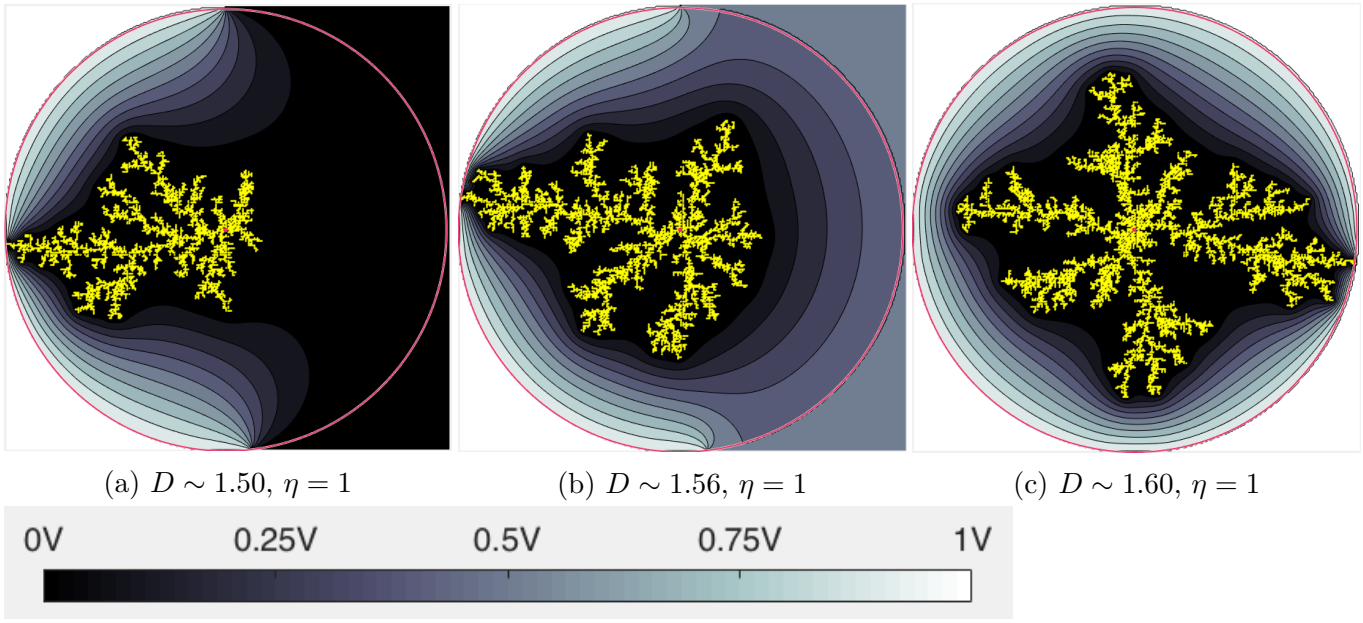

(a) $D \sim 1.50$, $\eta = 1$ (b) $D \sim 1.56$, $\eta = 1$ (c) $D \sim 1.60$, $\eta = 1$

Figure 3.15: These clusters were grown on a square lattice, with circular boundary conditions. In (a) the right half of the circumference was kept at $0V$, in (b) $0.5V$, and in (c) $1V$; the left half of the circumference was kept at $1V$ in all cases. The clusters are superimposed on a contour plot of the electric potential, defined by $E = -\nabla\Phi$.

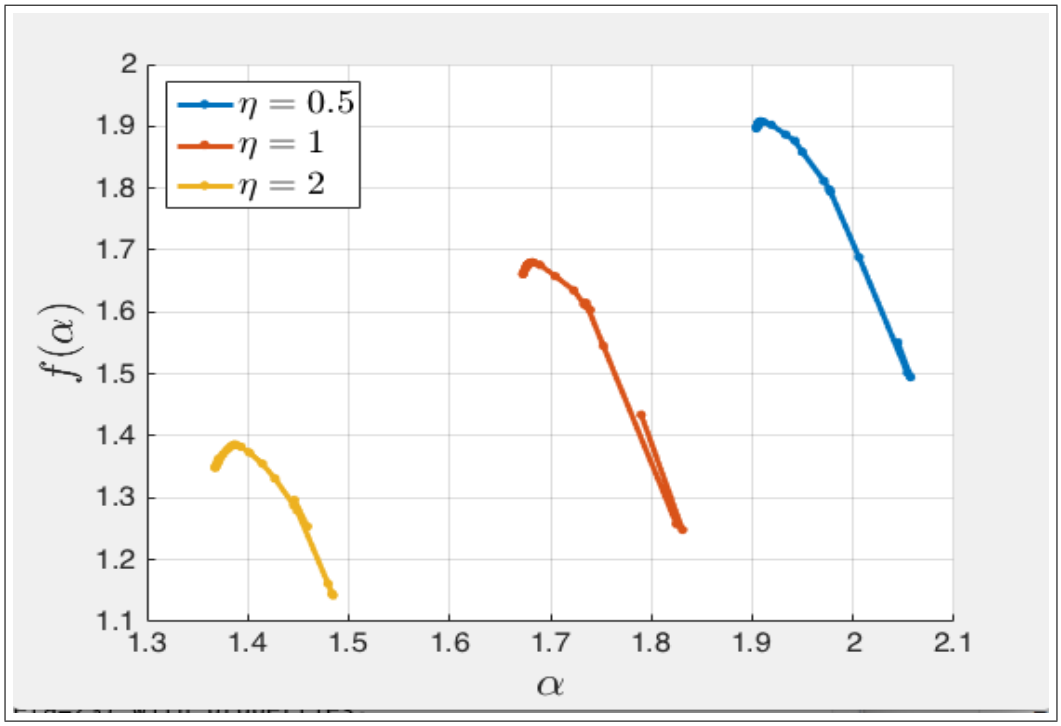

Figure 3.16: The singularity spectra (see section 2.9.1) of dielectric breakdown clusters grown on the square lattice with different values of η.

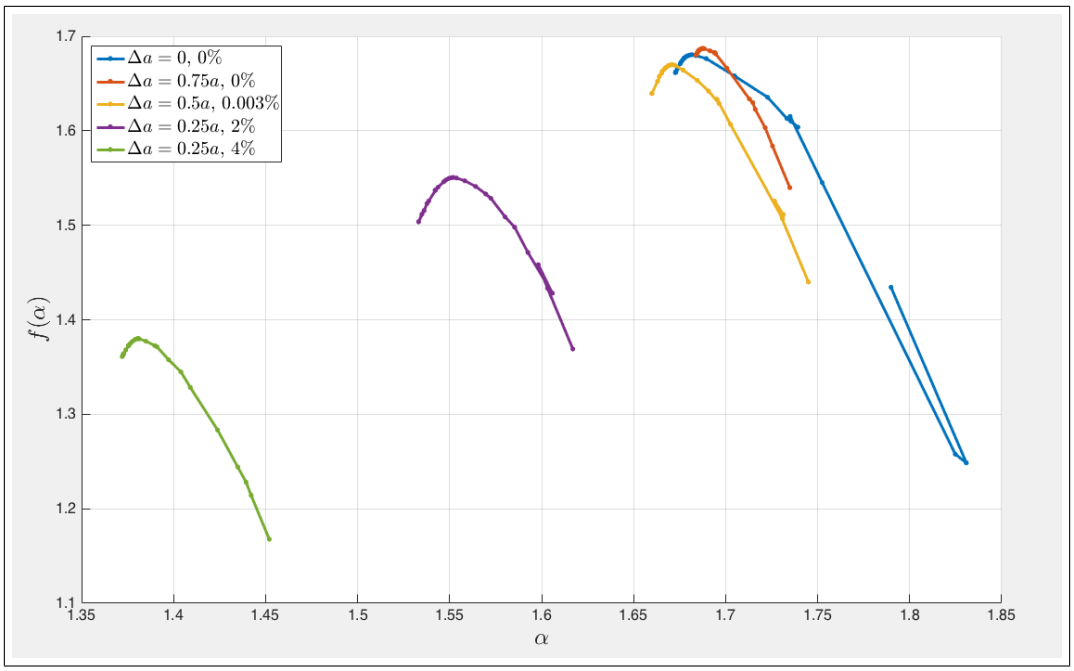

Figure 3.17: The singularity spectra (see section 2.9.1) of dielectric breakdown clusters grown on a random distribution of nodes with different values of neighbourhood shell size, Δa (see Fig. 2.3). The percentages are calculated as the number of nodes which have 0 nearest neighbours divided by the total number of nodes. Nodes with 0 nearest neighbours are electrically isolated from the rest of the distribution. The electric potential at these nodes is not updated, from an initial value, by the algorithm.

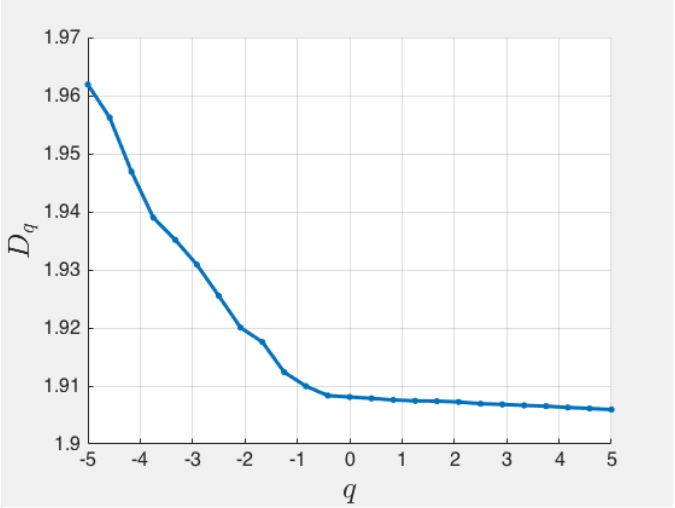

(a) Square lattice, $\eta = 0.5$.

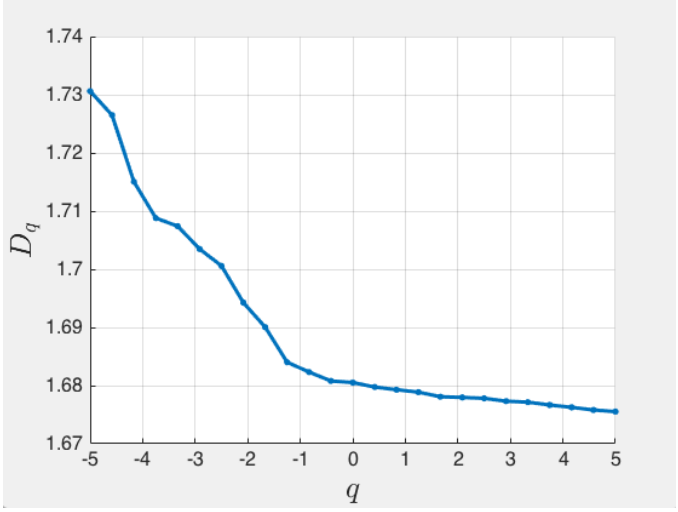

(b) Square lattice, $\eta = 1$

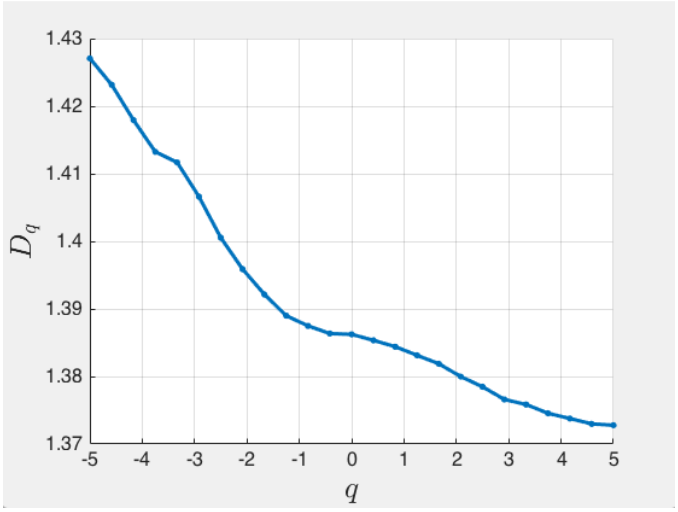

(c) Square lattice, $\eta = 2$

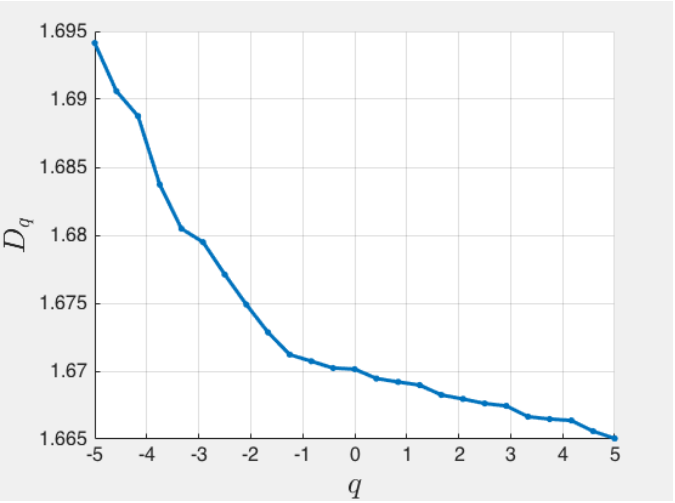

(d) Random distribution of nodes, $\eta = 1$, 0.003% of nodes with 0 n.n's

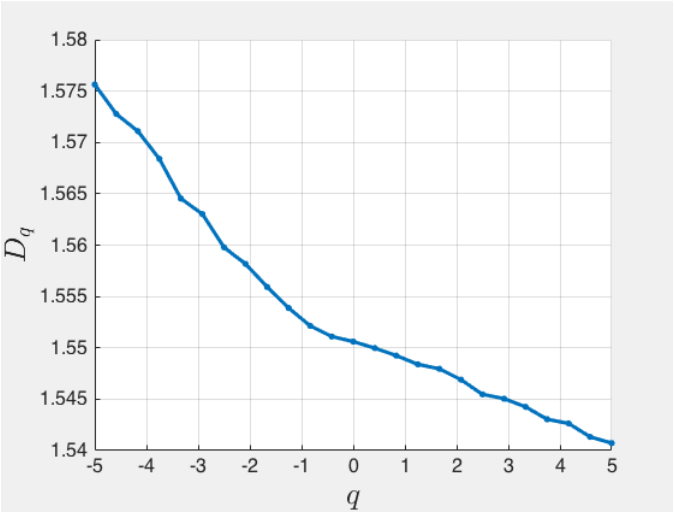

(e) Random distribution of nodes, $\eta = 1$, 2% of nodes with 0 n.n's

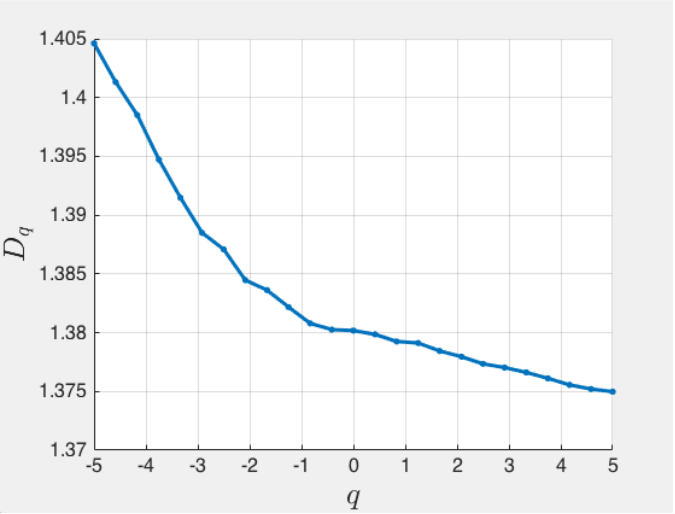

(f) Random distribution of nodes, $\eta = 1$, 4% of nodes with 0 n.n's

Figure 3.18: The generalized dimension, D_q, spectra for dielectric breakdown clusters. D_0 is the fractal dimension of the cluster.

Chapter 4

Conclusions

A general method to determine the resistance of any solid of revolution in cylindrical coordinates was created. The electric field, inside the types of resistors studied is not constant. The boundaries of the truncated resistors constrict the electric field non-uniformly, resulting in a non-uniform current density. This forces the current to flow between electrodes on curved paths, despite the divergence and curl of the field being zero. The deformation of a cylindrical element of current density within the resistor can be accounted for by the shear of $\vec{E}$. In general, the elements of the shear matrix are functions of (s, θ, z), however, for a cylindrical resistor, $\vec{E} = E\hat{z}$, each element is 0. The amount of bending of current flow lines depends on the ratio a/b; when $a/b \sim 1$ there is negligible bending, and the textbook method to find the resistance becomes more accurate. The current density increases rapidly near the smaller electrode when $a/b << 1$, causing significant bending of the current flow lines. The contribution to the total resistance can be accounted for by a spreading resistance term, $R_{spreading}$, such that $R = R_{bulk} + R_{spreading}$. The spreading resistance term in the total resistance dominates for $a/b << 1$, causing the textbook method (R_{bulk}) to underestimate the value for the total resistance.

The dielectric breakdown clusters are examples of statistical monofractals. They are self-similar over a finite range of length scales, and have uniform mass distributions that can be characterized by a single fractal dimension. This is indicated by the sharply peaked histograms in figure 3.11, the narrow $f(\alpha)$ spectra, constant D_q spectra, and the agreement between the sandbox and box counting methods. The fractal dimension, and appearance, of the clusters is unaffected by the number of nearest neighbours. On a random distribution of nodes the number of nearest neighbours locally varies. The fractal dimension is unaffected as long as the percentage of nodes with 0 nearest neighbours is close to 0%. When the percentage of nodes with 0 nearest neighbours increases the fractal dimension decreases, because nodes with 0 nearest neighbours are isolated from the rest of

the distribution and inhibit growth. This is due to regions of unusually low density preventing conduction of charge. The value of the exponent η, in the relationship between probability and electric field strength, the boundary conditions on the electric potential, and the density of the medium are the major factors which affect the fractal dimension.

Bibliography

[1] T. A. Witten and L. M. Sander. 1983. Diffusion-limited aggregation. Phys. Rev. B. 27(9):5686.

[2] David J. Griffiths. 1999. Introduction to Electrodynamics. Third Edition. Upper Saddle River (NJ): Pearson Education, Inc. Chapter 7, Electrodynamics; p. 333-334, Problem 7.40.

[3] J.D. Romano and R.H. Price. 1996. The Conical Resistor Conundrum: A Potential Solution. Am. J. Phys. 64(9):1150.

[4] R. S. Timsit. 1977. The potential distribution in a constricted cylinder. J. Phys. D: Appl. Phys. 10(15):2011 - 2019.

[5] J.D. Romano and R.H. Price. 2012. Why no shear in "Div, grad, curl, and all that"?. Am. J. Phys. 80(6):519.

[6] L. Niemeyer, L. Pietronero, and H. J. Wiesmann. 1984. Fractal Dimension of Dielectric Breakdown. Phys. Rev. Lett. 52(12):1033 - 1036.

[7] Sashi Satpathy. 1986. Dielectric breakdown in three dimensions: Results of numerical simulation. Phys. Rev. B. 33(7):5093 -5095.

[8] D.A. Willming and C. H. Wu. 1988. A stochastic model for dielectric breakdown in thin capacitors. J. Appl. Phys. 63:456.

[9] Rudolf H. Riedi (1999). Introduction to Multifractals. Dept. of ECE, Rice University. Retrieved from http://www.stat.rice.edu/ riedi/Publ/PDF/intro.pdf.

[10] Gerald L. Pollack and Daniel R. Stump. 2002. Electromagnetism. San Fransisco (CA): Pearson Education, Inc. Chapter 5, General Methods for Laplace's Equation; p. 133-135.

[11] Anders Bondeson, Thomas Rylander, and Pär Ingelström. 2005. Computational Electrodynamics. New York (NY): Spring Science+Business Media, Inc. Chapter 3, Finite Differences.

[12] Y. Sawada, S. Ohta, M. Yamazaki, and H. Honjo. 1982. Self-similarity and a phase-transition-like behavior of a random growing structure governed by a nonequilibrium parameter. Phys. Rev. A. 26(6):3557

[13] Tamas Vicszek. 1989. Fractal Growth Phenomena. Teaneck (NJ): World Scientific Publishing.

[14] Joseph Hoshen. 1997. Percolation and cluster structure parameters: The radius of gyration. J. Phys. A: Math Gen. 30(24):8459 - 8469.

[15] Tao Pang. 1997. An Introduction to Computational Physics. Cambridge (UK): Cambridge University Press. Chapter 2, Basic numerical methods; Chapter 6, Partial differential equations.

[16] L. Pietronero and E. Tosatti. 1985. Fractals in Physics. Amsterdam (NL): North-Holland Physics Publishing.